communications biology

Article

https://doi.org/10.1038/s42003-024-07052-1

Retinol binding protein 4 restricts PCV2 replication via selective autophagy degradation of viral ORF1 protein

Qingbing Han[1,2], Hejiao Zhao[1,2], Meng Chen[1,2], Wenshuo Xue[1,2], Jun Li[3], Lei Sun[4] & Yingli Shang[1,2,5]

Autophagy is a highly conserved degradative process that has been linked to various functions, including defending host cells against pathogens. Although the involvement of autophagy in porcine circovirus 2 (PCV2) infection has become apparent, it remains unclear whether selective autophagy plays a critical role in PCV2 restriction. Here we show that retinol-binding protein 4 (RBP4), an adipokine for retinol carrier, initiates the autophagic degradation of PCV2 ORF1 protein. PCV2 infection increases RBP4 protein levels through MAPK-eIF4E axis in living cells. Ectopic expression of RBP4 or recombinant RBP4 treatment promotes the degradation of ORF1 protein. Mechanistically, RBP4 activates TRAF6 to induce K63-linked ubiquitination of ORF1, leading to SQSTM1/p62-mediated selective autophagy for degradation. Consequently, RBP4 deficiency increases viral loads and exacerbates the pathogenicity of PCV2 in vivo. Collectively, these results identify RBP4 as a key host restriction factor of PCV2 and reveal a previously undescribed antiviral mechanism against PCV2 in infected cells.

Recifically interactedRetinol-binding protein 4 (RBP4) typically functions as a specific carrier for retinol in serum, which is mainly secreted by hepatocytes and adipocytes[1,2]. RBP4 levels are elevated in serum and adipose tissue in obesity-induced insulin resistance and are linked to other metabolic syndromes and cardiovascular diseases[3–5]. Notably, macrophages are also the major sites of RBP4 expression[6]. Several studies demonstrate that RBP4 expression can induce inflammatory responses in macrophages or endothelial cells through activation of toll-like receptor 4 (TLR4) or toll-like receptor 2 (TLR2)[7,8]. RBP4 expression is also correlated with infection by certain viruses. For example, RBP4 levels are increased during hepatitis C virus infection, and knockdown of RBP4 contributes to HCV replication[9]. In addition, RBP4 expression is also induced in vitro or in vivo in response to infection by several RNA viruses, including human immunodeficiency virus, influenza A virus, and porcine reproductive and respiratory syndrome virus[10–12]. However, the exact role of RBP4 in viral infection remains obscure.

Porcine circovirus type 2 (PCV2) is the primary causative agent of PCV-associated diseases (PCVDs) that lead to immense economic losses in the swine industry worldwide[13]. The genome of PCV2 is only ~1.7 kb in size and contains 11 predicated open reading frames (ORFs), with six of them having been well-characterized. Among these ORFs, ORF1 and ORF2 are the two main ones, encoding the replication-related protein (Rep) and the capsid protein (Cap), respectively[14]. Due to its small genome, PCV2 replication is considered to be heavily dependent on host cells[13]. Immune cells, including T and B lymphocytes, are the major targets of PCV2[15]. PCV2 also infects major antigen-presenting cells such as macrophages and dendritic cells. Eventually, PCV2 infection impairs the functions of target cells, which may contribute to PCV2 pathogenesis. It is believed that PCV2 may interact with host factors to modulate cell functions and viral infection[16]. Although numerous studies have investigated the pathogenesis of PCV2, the mechanisms by which PCV2 maintains persistent infection at a low level in target cells are poorly understood.

Autophagy is a highly conserved degradative process for clearance of cytosolic materials by the lysosomal pathway to maintain organismal homeostasis. It also acts as an important cell-autonomous defense mechanism against cytosolic microbes, especially viruses[17]. Particularly, selective autophagy degrades viral components or particles and modulates antiviral immune responses through the activation of cytosolic autophagy receptors that specifically bind cargoes and direct them to the autophagy machinery[18]. In fact, multiple

[1]Department of Preventive Veterinary Medicine, College of Veterinary Medicine, Shandong Agricultural University, Taian, Shandong, China. [2]Shandong Provincial Key Laboratory of Zoonoses, Shandong Agricultural University, Taian, Shandong, China. [3]Division of Swine Diseases, Shandong Provincial Key Laboratory of Animal Disease Control and Breeding, Institute of Animal Science and Veterinary Medicine, Shandong Academy of Agricultural Sciences, Jinan, China. [4]CAS Key Laboratory of Pathogenic Microbiology and Immunology, Institute of Microbiology, Chinese Academy of Sciences, Beijing, China. [5]Institute of Immunology, Shandong Agricultural University, Taian, Shandong, China. e-mail: shangyl@sdau.edu.cn

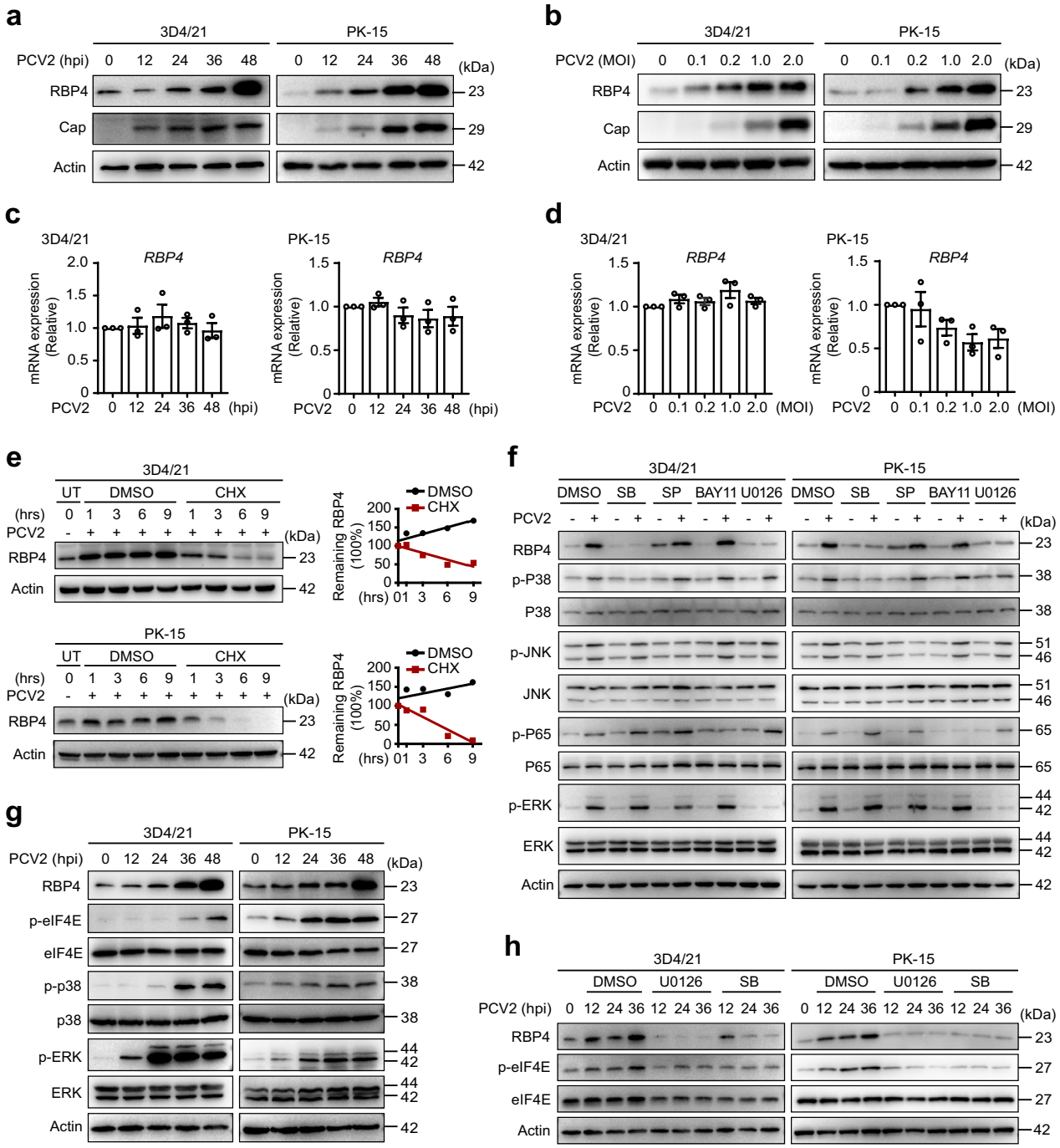

Fig. 1 | PCV2 infection induces RBP4 expression via the MAPK–eIF4E axis. Immunoblotting analysis of RBP4 protein levels and PCV2 capsid protein (Cap) expression in 3D4/21 cells and PK-15 cells infected with PCV2 (MOI = 0.2, the same dose below) at the indicated periods (**a**) or infected with PCV2 with increased dose for 36 h (**b**). Quantitative real-time PCR (qPCR) analysis of *RBP4* mRNA expression in 3D4/21 cells and PK-15 cells infected with PCV2 at the indicated periods (**c**) or infected with PCV2 with increased dose for 36 h (**d**). **e** Immunoblotting analysis of RBP4 protein expression in 3D4/21 cells and PK-15 cells left untreated or infected with PCV2 for 36 h following treatment with cycloheximide (CHX, 50 μM) for the indicated periods. Densitometric quantitation of RBP4 was normalized relative to the levels at 0 h conditions. **f** Immunoblotting analysis of RBP4, phosphorylated (p-) and total p38, p-JNK and JNK, p-p65 and p65, and p-ERK1/2 and ERK1/2 in whole lysates of in 3D4/21 cells or PK-15 cells pretreated with DMSO or p38 inhibitor SB203580 (SB, 10 μM), JNK inhibitor SP600125 (SP, 10 μM), NF-κB inhibitor BAY11 (10 μM), or ERK inhibitor U0126 (10 μM) for 3 h followed by PCV2 infection for 36 h. **g** Immunoblotting analysis of RBP4, phosphorylated (p-) and total eIF4E, p-p38 and p38, and p-ERK1/2 and ERK1/2 in whole lysates of 3D4/21 cells and PK-15 cells left untreated or infected with PCV2 for the indicated periods. **h** Immunoblotting analysis of RBP4, p-eIF4E, and total eIF4E in whole-cell lysates of 3D4/21 cells and PK-15 cells left untreated or pretreated with DMSO, U0126 (10 μM), or SB (10 μM) for 3 h followed by PCV2 infection for the indicated periods. Data are representative of three independent experiments (**a**, **b**, **e**–**h**) or pooled from three independent experiments (**c**, **d**, mean ± SD).

autophagy receptors, including SQSTM1/p62, OPTN, NDP52, NBR1, TOLLIP, and TAX1BP1, have been identified and are responsible for cargo recognition[18,19]. The process of cargo recognition typically involves the interaction of specific regions of the receptor with native cargo or with biochemical tags conjugated to the cargo. Among them, ubiquitin conjugated to cargo is a frequent tag recognized by autophagy receptors[20]. While autophagy functions as an efficient cell-intrinsic defense mechanism against invading pathogens, many

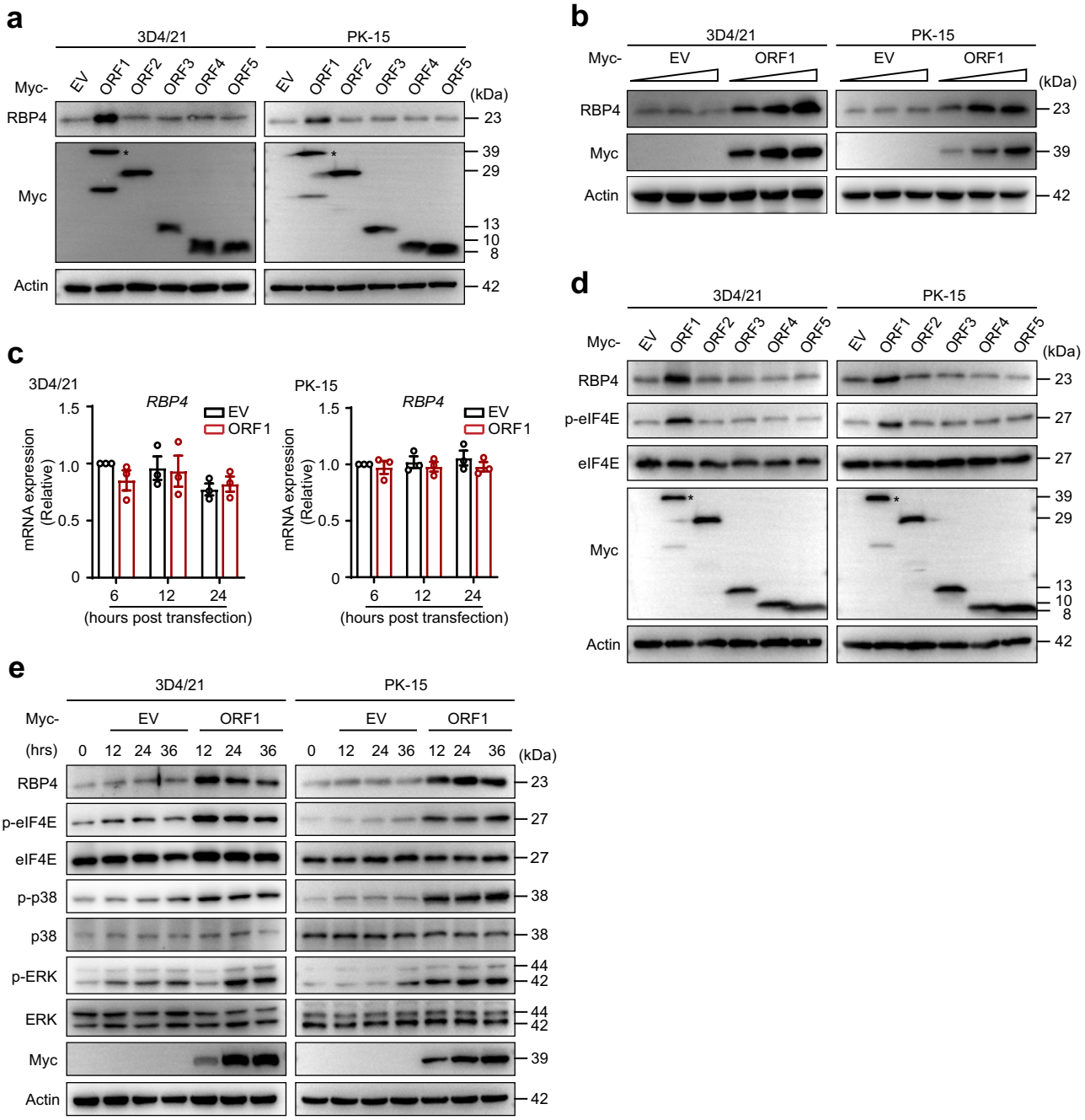

Fig. 2 | PCV2 ORF1 contributes to RBP4 induction and activation of MAPK–eIF4E. a Immunoblotting analysis of RBP4 and PCV2 ORF protein expression in whole-cell lysates of 3D4/21 cells and PK-15 cells transfected with empty vector (EV) or PCV2 ORF (ORF1–ORF5)-expressing plasmids for 24 h. **b** Immunoblotting analysis of RBP4 protein levels in whole-cell lysates of 3D4/21 cells and PK-15 cells transfected with EV or PCV2 ORF1-expressing plasmid with increased dose for 24 h. **c** qPCR analysis of *RBP4* mRNA levels in 3D4/21 cells and PK-15 cells transfected with EV or PCV2 ORF1 plasmid for the indicated periods. **d** Immunoblotting analysis of RBP4, p-eIF4E, and total eIF4E in whole-cell lysates of 3D4/21 cells and PK-15 cells transfected with EV or PCV2 ORF1-5 plasmids for 24 h. **e** Immunoblotting analysis of RBP4, p-eIF4E and total eIF4E, p-p38 and total p38, and p-ERK1/2 and total ERK1/2 in whole-cell lysates of 3D4/21 cells and PK-15 cells transfected with EV or PCV2 ORF1 plasmid for the indicated periods. Data are representative of three independent experiments (**a**, **b**, **d**, and **e**) or pooled from three independent experiments (**c**, mean ± SD).

viruses have evolved strategies to escape or exploit antiviral selective autophagy. For instance, autophagy receptors can bind to the ubiquitinated capsid proteins of chikungunya virus, the VP1 protein of foot-and-mouth disease virus, or the N protein of porcine epidemic diarrhea virus, targeting them to the autophagolysosome for degradation[21–23]. Pseudorabies virus tegument protein UL21 promotes cGAS degradation through TOLLIP-mediated selective autophagy[24]. Avibirnavirus VP3 can inhibit TRAF6-mediated NF-κB activation and interferon production to evade host innate immunity by SQSTM1/p62-mediated autophagic degradation[25]. Therefore, it is not surprising that viruses utilize the autophagy machinery to modulate their replication or infection.

In this study, we found that RBP4 protein levels are strikingly increased in response to PCV2 infection. Induction of RBP4, in turn, triggered the degradation of PCV2 ORF1 protein to repress viral replication. Moreover, we elucidated the mechanism by which RBP4

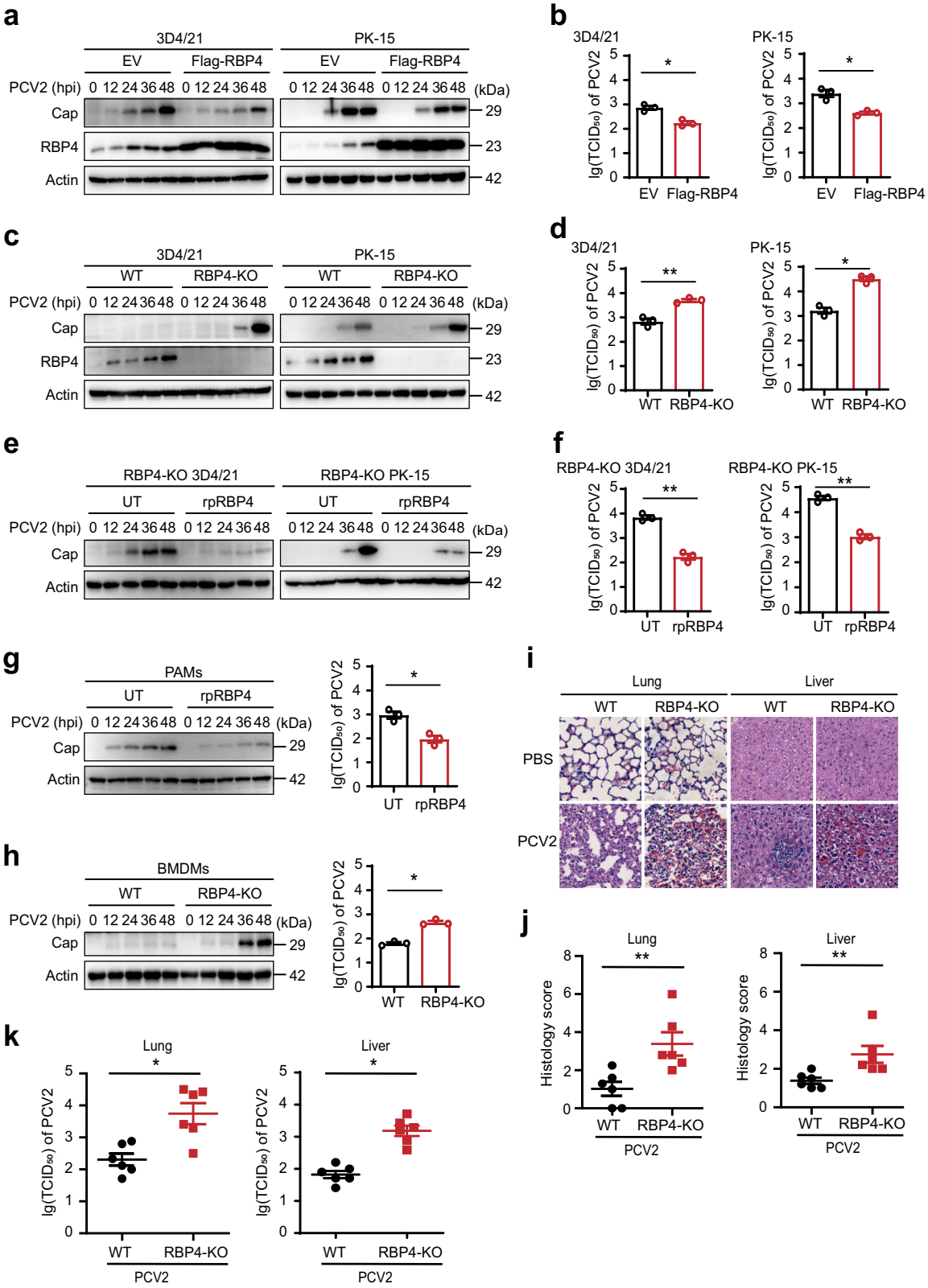

orchestrates selective autophagy against PCV2, which is mediated by TRAF6 and SQSTM1/p62. Hence, our results demonstrate that RBP4 is a key host restriction factor of PCV2 and uncover a previously uncharacterized host antiviral response that specifically initiates selective autophagic degradation of PCV2 ORF1 to suppress viral replication.

Results

PCV2 infection elevates RBP4 protein levels through the MAPK–eIF4E axis

The expression of adipokine RBP4 has recently been implicated in inflammatory responses and virus infection in macrophages or dendritic cells[7,8,12]. As we have previously shown that PCV2 infection can modulate

Fig. 3 | RBP4 inhibits replication of PCV2 in vitro and in vivo. Immunoblotting analysis of PCV2 Cap protein levels (**a**) or $TCID_{50}$ assay of viral titers (**b**) in 3D4/21 cells (left panel) or PK-15 (right panel) cells transfected with empty vector or Flag-RBP4 plasmid for 12 h followed by PCV2 infection for the indicated periods or 48 h. Immunoblotting analysis of PCV2 Cap protein levels (**c**) or $TCID_{50}$ assay of viral titers (**d**) in wild-type (WT) and RBP4-deficient (RBP4-KO) 3D4/21 cells (left panel), WT and RBP4-KO PK-15 cells (right panel) infected with PCV2 for indicated periods or 48 h. Immunoblotting analysis of PCV2 Cap protein levels (**e**) or $TCID_{50}$ assay of viral titers (**f**) in RBP4-KO 3D4/21 cells (left panel) and RBP4-KO PK-15 cells (right panel) infected with PCV2 for the indicated periods or 48 h. After 6 h of PCV2 infection, cells were treated with or without recombinant porcine RBP4 (rpRBP4, 30 μg/mL). **g** Immunoblotting analysis of PCV2 Cap protein levels (left panel) or $TCID_{50}$ assay of viral titers (right panel) in primary PAMs infected with PCV2 for the indicated periods or 48 h. After 6 h of PCV2 infection, the cells were treated with or without recombinant porcine RBP4 (rpRBP4, 30 μg/mL). **h** Immunoblotting analysis of PCV2 Cap protein levels (left panel) or $TCID_{50}$ assay of viral titers (right panel) in WT or RBP4-KO BMDMs infected with PCV2 for the indicated periods or 48 h. **i** Hematoxylin and eosin (H&E) staining of lung (left) and liver (right) sections from mice infected with PCV2 (5×10^5 pfu/mouse) for 7 days. Scale bar, 20 μm. Original magnification, ×40. **j** Histological scores of lung and liver from mice infected by PCV2 as in (**i**). Each symbol represents an individual mouse ($n = 6$/group). **k** Viral titers in the lung (left) and liver (right) from WT and RBP4-KO mice ($n = 6$/group) infected with PCV2 in (**i**). Data are pooled from three independent experiments (**b**, **d**, **f** and **g**, **h** right, **j**, **k**, mean ± SD) or representative of three independent experiments (**a**, **c**, **e** and **g**, **h** left, **i**). $^*p < 0.05$, $^{**}p < 0.01$ (Student's *t* test).

macrophage functions that contribute to viral pathogenesis[15], we next sought to determine if RBP4 is also related to PCV2 infection. Therefore, we examined the mRNA and protein levels of RBP4 in porcine alveolar macrophages (3D4/21 cells) and porcine kidney cells (PK-15 cells) infected with PCV2. While PCV2 infection significantly increased RBP4 protein levels in both 3D4/21 cells and PK-15 cells at multiple indicated periods (Fig. 1a, b). PCV2 infection did not obviously alter the mRNA expression of *RBP4* (Fig. 1c, d). These data indicate that PCV2 infection likely induces increases in RBP4 protein at post-transcriptional levels. To examine this, RBP4 protein levels were monitored in PCV2-infected macrophages or PK-15 cells treated with cycloheximide (CHX), a well-known protein synthesis inhibitor. We found that induction of RBP4 protein mediated by PCV2 was abolished after CHX treatment (Fig. 1e, upper), and RBP4 protein decayed faster in CHX-treated cells than that in control cells (Fig. 1e, lower). These data suggest that RBP4 induction by PCV2 is possibly due to new protein synthesis.

It has been reported that PCV2 infection activates multiple signaling pathways, including MAPK and NF-κB signals[15]. To determine which signals are involved in the regulation of RBP4 during PCV2 infection, we treated cells with multiple chemical inhibitors, including SB203580(SB), SP600125(SP), Bay11, or U0126, for targeting different signaling pathways. Treatment with these chemical inhibitors effectively suppressed the phosphorylation of p38, JNK, p65, or ERK induced by PCV2 infection in both 3D4/21 and PK-15 cells, indicating that the chemical inhibitors are effective at the concentration in use (Fig. 1f). Notably, inhibition of p38 and ERK–MAPKs, but not NF-κB or JNK, suppressed the induction of RBP4 protein mediated by PCV2 infection (Fig. 1f), demonstrating that activation of the p38 and ERK–MAPK signaling pathways is correlated with RBP4 protein induction. Indeed, phosphorylation of p38 and ERK was observed in PCV2-infected 3D4/21 cells and PK-15 cells at multiple periods (Fig. 1g). It has been established that the eukaryotic translation initiation factor 4E (eIF4E) plays critical roles in the initiation of translation, and phosphorylation of eIF4E is orchestrated by activation of MAPKs[26]. Therefore, we examined the activation of eIF4E in PCV2-infected cells and found that PCV2 infection also promoted eIF4E phosphorylation in 3D4/21 and PK-15 cells (Fig. 1g), the downstream signal of phosphorylation of p38 and ERK–MAPK, demonstrating that PCV2-mediated induction of RBP4 is likely dependent on eIF4E activation. In line with this notion, induction of RBP4 by PCV2 was abolished when cells were treated with chemical inhibitors of p38 and ERK–MAPK, which significantly suppressed the phosphorylation of eIF4E without altering the expression of total eIF4E (Fig. 1h), indicating that the MAPK–eIF4E axis is critical for induction of RBP4 by PCV2. Together, these results suggest that PCV2 infection elevates RBP4 protein levels likely through activation of the MAPK–eIF4E axis.

PCV2 ORF1 contributes to RBP4 induction and MAPK–eIF4E activation

Next, we sought to determine which viral components are responsible for RBP4 protein induction. We transfected expression plasmids for PCV2 ORFs in both 3D4/21 cells and PK-15 cells and found that PCV2 ORF1, but not PCV2 ORF2 to ORF5, strongly induced RBP4 protein expression (Fig. 2a). Moreover, PCV2 ORF1 increased RBP4 protein levels in a dose-dependent manner (Fig. 2b). In addition, PCV2 ORF1 did not affect the mRNA expression of *RBP4* (Fig. 2c). These results demonstrate that the expression of PCV2 ORF1 plays a pivotal role in RBP4 protein induction. Considering that PCV2 infection promoted activation of the MAPK–eIF4E signaling pathway to elevate RBP4 protein levels, we then examined whether ORF1 expression contributes to the activation of the MAPK–eIF4E axis. Not surprisingly, PCV2 ORF1 but not the other PCV2 ORFs (ORF2–ORF5), promoted phosphorylation of p38 and ERK–MAPK, as well as phosphorylation of eIF4E, in both 3D4/21 cells and PK-15 cells (Fig. 2d, e). Taken together, these results suggest that PCV2 ORF1 is the key viral component leading to RBP4 induction via the MAPK–eIF4E axis.

RBP4 inhibits the replication of PCV2 in vitro and in vivo

Next, we addressed whether RBP4 expression affects PCV2 replication in RBP4-deficient cells or in RBP4-deficient mice in vivo (Supplementary Fig. 1). Indeed, ectopic expression of RBP4 suppressed PCV2 replication in both 3D4/21 cells and PK-15 cells, as shown by PCV2 Cap protein expression, viral titers and PCV2 DNA copies (Fig. 3a, b and Supplementary Fig. 2a, b), suggesting that RBP4 functions as a negative regulator of PCV2 replication. To further confirm the regulatory functions of RBP4 during PCV2 infection, we generated RBP4-deficient 3D4/21 cells and PK-15 cells using a CRISPR-Cas9-based approach. As expected, deficiency of RBP4 substantially promoted PCV2 replication in 3D4/21 cells and PK-15 cells (Fig. 3c, d and Supplementary Fig. 2c, d), supporting the notion that RBP4 acts as a restriction factor for PCV2. RBP4 is a secreted cytokine that acts through its membrane receptors in macrophages[7]. To avoid the endogenous RBP4 effect, we stimulated RBP4-deficient 3D4/21 cells or RBP4-deficient PK-15 cells with exogenous recombinant porcine RBP4 (rpPBP4) and found that rpRBP4 significantly suppressed PCV2 replication (Fig. 3e, f and Supplementary Fig. 2e, f). Additionally, rpRBP4 also inhibited the replication of PCV2 in primary porcine alveolar macrophages (Fig. 3g and Supplementary Fig. 2g), further suggesting that RBP4 is a restriction factor of PCV2 replication. Similarly, deficiency of RBP4 in murine bone marrow-derived macrophages (BMDMs) accelerated PCV2 replication (Fig. 3h and Supplementary Fig. 2h). In summary, these data suggest that RBP4 represses PCV2 replication in vitro.

To investigate whether such a phenomenon occurs in vivo, we challenged wild-type and RBP4-deficient mice with PCV2 by intraperitoneal injection. Histological analysis of lung and liver tissues revealed severe signs of inflammation and hemorrhage in RBP4-deficient mice relative to that of wild-type mice infected with PCV2 (Fig. 3i, j), indicating that RBP4 deficiency weakened host defenses against PCV2. Meanwhile, the viral titers and PCV2 DNA copies were significantly lower in tissues from wild-type mice than those from RBP4-deficient mice (Fig. 3k and Supplementary Fig. 2i). Collectively, these data demonstrate that RBP4 also restricts PCV2 replication in vivo.

RBP4 promotes autophagic degradation of PCV2 ORF1

Having uncovered that RBP4 is a host restriction factor for PCV2, we next sought to investigate the mechanisms by which RBP4 suppresses PCV2

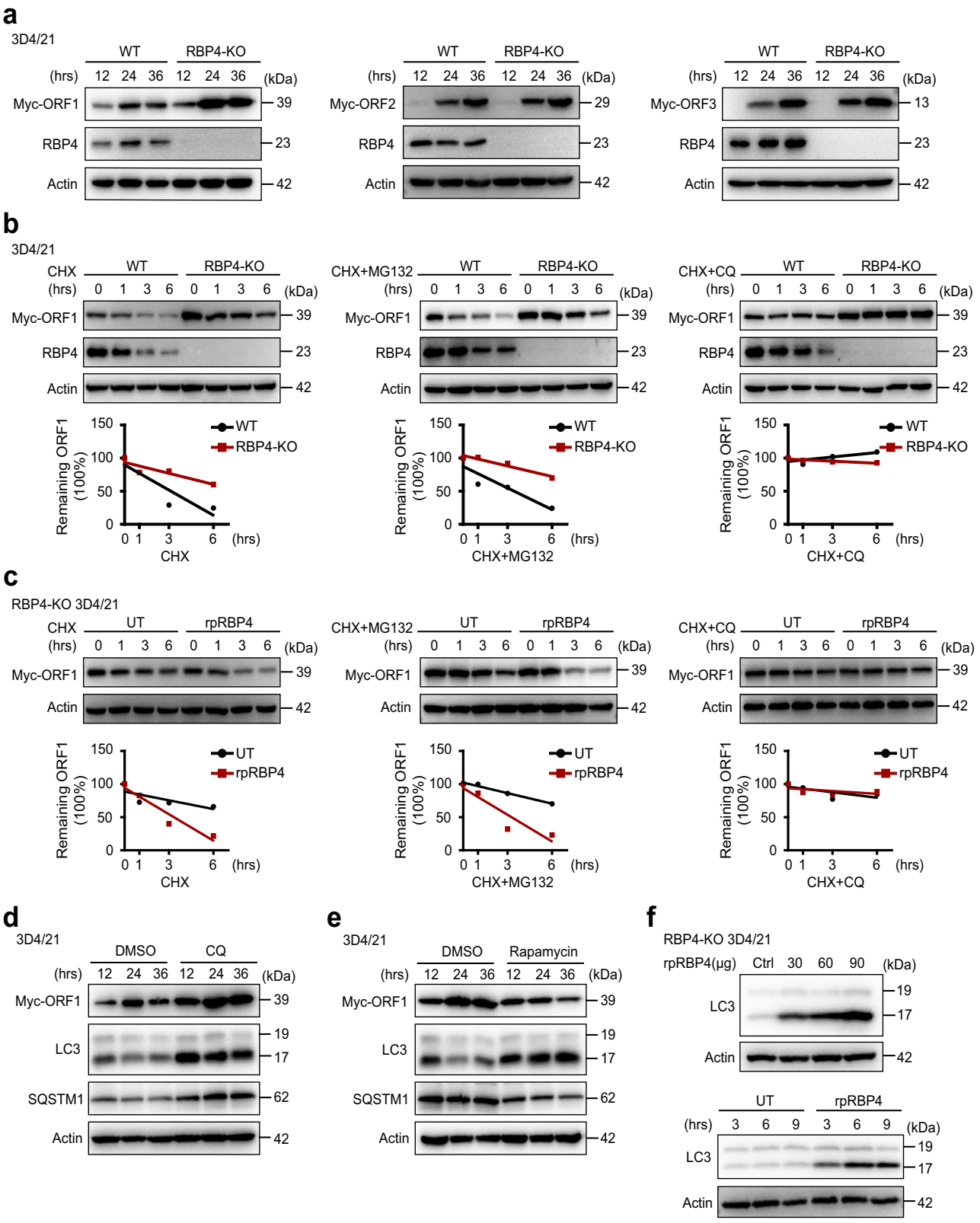

replication. Type I interferon (IFN) and its downstream IFN-stimulated genes (ISGs) plays a crucial role in host antiviral immune responses to limit viral replication. Considering that RBP4 contributes to the expression of inflammatory cytokines in macrophages[27], we first examined whether RBP4 regulates the expression of *IFNB1*, *TNFa*, and *MX1*. qPCR analysis revealed that *IFNB1*, *TNFa*, and *MX1* expression was comparable in wild-type and RBP4-deficient 3D4/21 cells, PK-15 cells, or murine BMDMs in response to pattern recognition receptor ligand stimulation (Supplementary Fig. 3), suggesting that RBP4 deficiency does not alter expression of IFN.

We next determined whether RBP4 suppresses the expression of key viral components of PCV2. Notably, the protein expression of ORF1 but not ORF2 and ORF3 was more pronounced in RBP4-deficient cells than that in

Fig. 4 | RBP4 promotes autophagic degradation of PCV2 ORF1.
a Immunoblotting analysis of Myc-tagged protein expression of PCV2 ORF1 (left), ORF2 (middle), or ORF3 (right) in whole-cell lysates of WT and RBP4-KO 3D4/21 cells transfected with the expression plasmids for the indicated periods, respectively. **b** Immunoblotting analysis of PCV2 ORF1 protein levels in whole-cell lysates of WT and RBP4-KO 3D4/21 cells transfected with PCV2 ORF1 expression plasmid for 24 h following treatment with CHX alone (left) (50 μM), CHX together with MG-132 (middle) (30 μM), or CHX together with CQ (right) (20 μM) for the indicated times. Densitometric quantitation of PCV2 ORF1 was normalized relative to the levels of 0 h conditions (**b**, lower). **c** Immunoblotting analysis of PCV2 ORF1 protein expression in whole-cell lysates of RBP4-KO 3D4/21 cells transfected with the PCV2 ORF1 expression plasmid for 24 h and then left untreated or stimulated with rpRBP4 protein (30 μg/mL) for 1 h following treatment with CHX alone, CHX together with MG132, or CHX together with CQ for the indicated times. Densitometric quantitation of PCV2 ORF1 was normalized relative to the levels at 0 h conditions (**c**, lower). Immunoblotting analysis of PCV2 ORF1 protein expression in 3D4/21 cells transfected with PCV2 ORF1 expression plasmid for 6 h following treatment with CQ (20 μM) (**d**) or rapamycin (1 μM) (**e**) for the indicated periods. **f** Immunoblotting analysis of LC3 expression in RBP4-KO 3D4/21 cells stimulated with rpRBP4 with increased dose for 6 h (upper) or stimulated with rpRBP4 protein (30 μg/mL) for indicated periods (lower). Data are representative of three (**a**, **d**, **e**) or two (**b**, **c**, **f**) independent experiments.

wild-type cells (Fig. 4a and Supplementary Fig. 4a), indicating that RBP4 deficiency facilitates ORF1 protein expression. Specifically, we found that ORF1 protein levels displayed a rapid reduction in wild-type cells compared to RBP4-deficient cells when cells were treated with CHX, indicating that RBP4 may impair the stability of ORF1 (Fig. 4b and Supplementary Fig. 4b, left). To further clarify this observation, we examined the ORF1 protein stability in cells treated with chemical inhibitors of the proteasome or lysosomal degradation pathways[28]. We found that the proteasome inhibitor MG-132 did not retard ORF1 degradation after termination of protein synthesis by CHX in both wild-type and RBP4-deficient cells (Fig. 4b and Supplementary Fig. 4b, middle). In contrast, the lysosomal inhibitor chloroquine (CQ) prevented ORF1 degradation after CHX treatment in both wild-type and RBP4-deficient cells (Fig. 4b and Supplementary Fig. 4b, right), indicating that RBP4 promoted degradation of ORF1 protein through the autophagy-lysosomal pathway. This notion was further corroborated by adding exogenous recombinant RBP4 (rRBP4) protein to RBP4-deficient cells treated with CHX and CQ, showing that rRBP4 treatment accelerates degradation of ORF1 protein (Fig. 4c and Supplementary Fig. 4c). Moreover, inhibition of autophagy by CQ markedly increased ORF1 protein expression (Fig. 4d and Supplementary Fig. 4d, e), whereas the autophagy stimulator rapamycin counteracted the increase in ORF1 in 3D4/21 cells and HeLa cells transfected with myc-ORF1 (Fig. 4e and Supplementary Fig. 4d, f). In addition, rpRBP4 treatment increased the levels of LC3-II in a dose- and time-dependent manner in RBP4-deficient 3D4/21 cells (Fig. 4f), supporting that RBP4 expression can initiate autophagy process. Collectively, these data suggest that RBP4 can promote degradation of ORF1 protein through the autophagy-lysosomal pathway.

SQSTM1/p62-mediated autophagy is responsible for PCV2 ORF1 degradation

Selective autophagy typically targets specific, often potentially harmful, cargoes for degradation. Previous studies suggest that cargo receptors, including SQSTM1/p62, NBR1, NDP52, OPTN, TOLLIP, and TAX1BP1 are responsible for substrate delivery to autophagosomes for selective degradation[18,19]. To determine if ORF1 is degraded through selective autophagy and which cargo receptors are involved, we performed immunoprecipitation by transfecting Myc-ORF1 and GFP-tagged SQSTM1/p62, NBR1, NDP52, OPTN, TOLLIP, or TAX1BP1 in 3D4/21 cells. We found that ORF1 specifically interacted with SQSTM1/p62 but not other cargo receptors (Fig. 5a and Supplementary Fig. 5a), demonstrating that SQSTM1/p62 serves as the cargo receptor for PCV2 ORF1 degradation. The interaction between ORF1 and endogenous SQSTM1/p62 was also reproducible in 3D4/21 cells (Fig. 5b). Moreover, immunofluorescence assays also demonstrated that ORF1 co-localizes with exogenous SQSTM1/p62 in 3D4/21 cells (Fig. 5c), further supporting the interaction between ORF1 and SQSTM1/p62.

Selective autophagy receptors are equipped with a ubiquitin-binding domain (UBD) and LC3 interacting region (LIR), which allow them to physically bridge cargo to autophagosomes[29]. Indeed, SQSTM1/p62 facilitates the recruitment of LC3 to the ubiquitylated proteins for degradation in autophagosomes. Interestingly, PCV2 ORF1 specifically interacted with LC3 in both 3D4/21 cell and HeLa cells (Fig. 5d). Consistently, confocal immunofluorescence also showed strong colocalization of ORF1 or SQSTM1/p62 puncta with LC3 (Fig. 5e), indicating that PCV2 ORF1 is likely targeted to autophagosomes through interaction with SQSTM1/p62 and LC3. Importantly, knockdown of SQSTM1/p62 but not other cargo receptors impaired the interaction and colocalization of PCV2 ORF1 with LC3 (Fig. 5f, g and Supplementary Fig. 5b), suggesting that SQSTM1/p62 acts as a bridge for ORF1 and LC3 interaction and plays a predominant role in selective autophagy-mediated degradation of ORF1. We next determined whether ORF1 degradation is dependent on SQSTM1/p62. Indeed, we found that SQSTM1/p62 knockdown slowed ORF1 degradation in the presence of CHX (Fig. 5h). Altogether, the above data suggest that SQSTM1/p62 is responsible for the colocalization and interaction of ORF1 with LC3 and the subsequent selective autophagic degradation of ORF1.

RBP4 activates TRAF6 to promote PCV2 ORF1 K63-linked ubiquitination

As SQSTM1/p62 generally recruits ubiquitin-conjugated substrates to autophagosomes[30], we next investigated whether RBP4 modulates SQSTM1/p62-mediated ORF1 ubiquitination. We found that RBP4 deficiency remarkably suppresses ORF1 ubiquitination in 3D4/21 cells and HeLa cells, which impaired K63-linked ubiquitination of ORF1 but not that of K6, K11, K27, K29, K33 or K48-linked ubiquitination (Fig. 6a and Supplementary Fig. 6a). The results suggest that RBP4 is responsible for ORF1 K63-linked polyubiquitination. Consistently, rRBP4 protein treatment substantially promoted K63- but not K48-linked ubiquitination of ORF1 in RBP4-deficient cells and failed to induce ORF1 ubiquitination in the presence of a K63R mutant, in which lysine at position 63 was mutated to arginine (Fig. 6b and Supplementary Fig. 6b), further supporting that RBP4 induces K63-linked ubiquitination of ORF1.

TNF receptor associated factor 6 (TRAF6) is the key E3 ligase for K63-linked ubiquitination of target proteins during TLR4-induced autophagy[31]. We therefore sought to determine if TRAF6 is also responsible for K63-linked ubiquitination of PCV2 ORF1. Immunoprecipitation assays revealed that GFP-tagged TRAF6 indeed interacts with PCV2 ORF1 but not ORF1 of PCV3 or PCV4, indicating a relatively specific interaction between TRAF6 and PCV2 ORF1 in 3D4/21 cells and HeLa cells (Fig. 6c and Supplementary Fig. 6c). Moreover, confocal microscopy analysis showed that PCV2 ORF1 co-localizes with TRAF6 (Fig. 6d and Supplementary Fig. 6d). To know whether there is direct interaction between PCV2 ORF1 and TRAF6, LC3, or SQSTM1/p62, we expressed and purified recombinant proteins of GST-tagged TRAF6, LC3 and SQSTM1/p62, as well as recombinant PCV2-ORF1 with a His tag for pull-down assay in vitro. The results showed that ORF1 can bind to GST-TRAF6 directly but not to GST-SQSTM1/p62 or GST-LC3 (Fig. 6e), suggesting that ORF1 directly interacts with TRAF6 instead of SQSTM1/p62 or LC3. Next, we determined the mechanisms of how TRAF6 specifically binds to PCV2 ORF1. Analysis of the structural determinants of protein-TRAF6 interaction reveals a (Pro-X-Glu-X-X-Aromatic/Acidic, Pro-X-Glu-X-X-Ar/Ac) TRAF6-binding motif[32]. Therefore, we searched for a potential Pro-X-Glu-X-X-Ar/Ac motif in the ORF1 protein of PCV viruses and found that only PCV2 ORF1 contains a conserved TRAF6-binding motif (Fig. 6f). Indeed, double mutants of PCV2 ORF1 targeting the key residues in the TRAF6-binding motif lost the ability to interact with TRAF6 (Fig. 6g), demonstrating that PCV2 ORF1 interacts with TRAF6 through the TRAF6-binding motif.

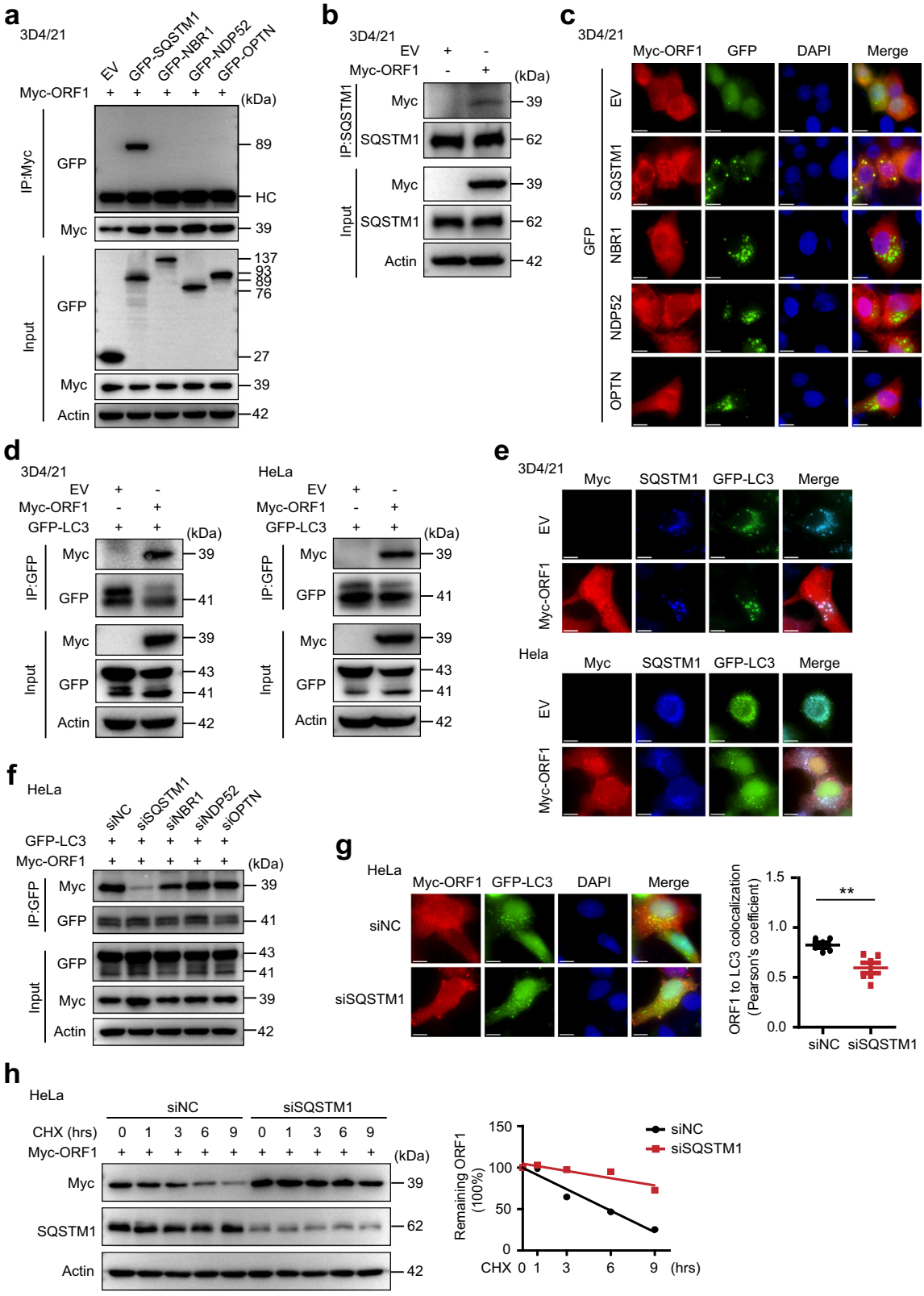

To determine whether TRAF6 activates the K63-linked ubiquitination of PCV2 ORF1, we performed immunoprecipitation by transfecting 3D4/21 cells with GFP-TRAF6, Myc-ORF1, and His-ubiquitin (His-Ub) or His-ubiquitin mutants. Indeed, TRAF6 expression substantially increased total and K63-linked ubiquitination of ORF1 but not other types of ubiquitination of ORF1 (Fig. 6h), demonstrating that TRAF6 is the E3 ligase for K63-linked ubiquitination of ORF1. Conversely, knockdown of TRAF6 substantially attenuated K63-linked ubiquitination induced by exogenous rRBP4 in RBP4-deficient cells (Fig. 6i), confirming that TRAF6 is critical for K63-linked ORF1 ubiquitination. Taken together, these data suggest that RBP4 promotes TRAF6-mediated K63-linked ubiquitination and degradation of ORF1 via selective autophagy.

Fig. 5 | SQSTM1/p62-mediated autophagy is responsible for PCV2 ORF1 degradation. a Immunoblotting analysis of the indicated proteins in immunoprecipitated (IP) samples and whole-cell lysates of 3D4/21 cells transfected with PCV2 ORF1 (Myc-tagged) together with pEGFP-C1 empty vector, GFP-SQSTM1/p62, GFP-NBR1, GFP-NDP52, or GFP-OPTN for 24 h. **b** Immunoblotting analysis of endogenous SQSTM1 and PCV2 ORF1 in immunoprecipitated samples or whole-cell lysates of 3D4/21 cells transfected with empty vector (EV) or the PCV2 ORF1 expression plasmid. Anti-SQSTM1 immunoprecipitates or levels of the indicated proteins in whole-cell lysates were analyzed by immunoblotting with anti-Myc antibody or anti-SQSTM1 antibody. **c** Colocalization of PCV2 ORF1 (red) and SQSTM1, NBR1, NDP52, or OPTN (green) in 3D4/21 cells transfected with PCV2 ORF1 together with pEGFP-C1 empty vector, GFP-SQSTM1, GFP-NBR1, GFP-NDP52, or GFP-OPTN for 24 h. Scale bar, 10 μm. **d** Immunoprecipitation analysis of the association of PCV2 ORF1 and LC3 in 3D4/21 cells (left) or HeLa cells (right) transfected with PCV2 ORF1 and GFP-LC3 plasmids for 24 h. **e** Colocalization of PCV2 ORF1 (red), SQSTM1 (blue), and LC3 (green) in 3D4/21 (upper) and HeLa cells (lower). Cells were transfected with PCV2 ORF1 and GFP-LC3 for 12 h following treatment with CQ (20 μM) for another 12 h before confocal microscopy. Endogenous SQSTM1 was labeled by anti-SQSTM1 antibody. **f** Immunoprecipitation analysis of association of PCV2 ORF1 with LC3 in HeLa cells transfected with siRNA oligos specifically targeting SQSTM1/p62 (SQSTM1 siRNA), NBR1 (NBR1 siRNA), NDP52 (NDP52 siRNA), OPTN (OPTN siRNA), or control siRNA oligos (Control siRNA) (100 nM). Twenty-four hours after transfection, cells were further transfected with PCV2 ORF1 and GFP-LC3 plasmids for another 24 h before analysis. **g** Colocalization of PCV2 ORF1 (red) and LC3 (green) in HeLa cells transfected with siRNA targeting SQSTM1/p62 or control siRNA oligos (100 nM). Twenty-four hours after transfection, cells were further transfected with PCV2 ORF1 and GFP-LC3 plasmids for another 12 h followed by treated with CQ (20 μM) for another 12 h before analysis. Pearson's correlation coefficient analysis was based on multiple sight fields in each group ($n = 6$ fields). **h** Immunoblotting analysis of PCV2 ORF1 protein and SQSTM1/p62 expression in whole-cell lysates of HeLa cells transfected with siRNA targeting SQSTM1/p62 or control siRNA oligos (100 nM). Twenty-four hours after transfection, cells were further transfected with PCV2 ORF1 for another 24 h following treatment with CHX (50 μM) for the indicated times. Densitometric quantitation of PCV2 ORF1 was normalized relative to the levels at 0 h conditions (**h**, right). Data are representative of three (**a**–**e**, **g**) or two (**f**, **h**) independent experiments or are pooled from three independent experiments (**g**, right). $^{**}p < 0.01$, (Student's *t* test).

TRAF6 interacts with ORF1 to modulate its degradation

Structurally, PCV2 ORF1 contains three key domains: an N-terminal endonuclease domain (ED), an oligomerization domain (OD) in the middle, and a C-terminal ATPase domain (AD)[33]. To map the key functional domains of ORF1 that interact with TRAF6 and SQSTM1/p62, we generated three ORF1 mutants: ORF1-ED (ED domain only, aa 1–118), ORF1-AD (AD domain only, aa 158–314), and ORF1-ΔOD (OD domain deletion, aa 119–157). Immunoprecipitation assays demonstrated that ORF1-AD was sufficient to interact with TRAF6 (Fig. 7a, b). Similarly, ORF1-AD is indispensable for the colocalization between ORF1 and TRAF6 (Fig. 7c). However, neither ORF1-ED nor ORF1-AD interacted with SQSTM1/p62, and deletion of the OD region did not hamper the interaction between ORF1 and SQSTM1/p62 (Fig. 7d). These results suggest that the interaction between SQSTM1/p62 and ORF1 possibly relies on the concurrent presence of both the ED and AD regions. This notion was further verified by immunoprecipitation assays showing that both the ED and AD domains are critical for TRAF6-mediated ubiquitination of ORF1 (Fig. 7e). As SQSTM1/p62 is an ubiquitin-dependent autophagy receptor that recognize the ubiquitin chain[18], TRAF6 may directly interact with the ORF1-AD, and SQSTM1/p62 may bind to the ubiquitin chain in the ORF1-ED. To strengthen this conclusion, we generated a series of ORF1 mutants containing one lysine residue only at position 4, 5, 15, 30, 31, 66, 67, 72, 74, 85, 87, 94, or 99, or a mutant (ORF1 ED-AKR) in which all lysine residues were substituted for arginine. Immunoprecipitation assays demonstrated that TRAF6 expression predominantly induced the ubiquitination of ORF1 at positions 15, 66, 67, 94, or 99 (Fig. 7f, g), indicating that these five lysine residues of ORF1 are responsible for TRAF6-mediated polyubiquitination. Taken together, these results indicate that TRAF6 mediates polyubiquitination and degradation of ORF1 at multiple lysine sites.

TLR4 is critical for RBP4-mediated ubiquitination of ORF1 in macrophages

Retinol-free RBP4 promotes inflammatory responses by binding to the toll-like receptors (TLR4) in macrophages[27]. Because RBP4 expression inhibits PCV2 replication, we therefore examined whether RBP4 functions as a secreted cytokine to activate TLR signaling to suppress PCV2 replication. Indeed, ectopic expression of exogenous RBP4 can lead to the secretion of RBP4 protein into the supernatant of RBP4-deficient 3D4/21 cells, and RBP4 expression strikingly suppressed PCV2 replication (Fig. 8a). To further determine whether TLR4 is essential for RBP4 to suppress PCV2 replication, TAK242, a known selective antagonist of TLR4, was applied to RBP4-deficient 3D4/21 cells[7]. We found that TAK242 treatment elevated the protein levels of PCV2 Cap (Fig. 8a), DNA copies of PCV2 and viral titers (Fig. 8b), suggesting that TLR4 is crucial for RBP4 to modulate PCV2 replication. To determine whether TAK242 treatment affects RBP4-mediated ubiquitination of ORF1, we performed immunoprecipitation by transfecting with FLAG-RBP4, Myc-ORF1, and His-ubiquitin-K63 (His-Ub-K63) in RBP4-deficient 3D4/21 cells with or without TAK242 treatment. As expected, TAK242 treatment blocked RBP4-induced K63-linked polyubiquitination of ORF1 (Fig. 8c), suggesting that TLR4 is critical for RBP4 to mediate ORF1 ubiquitination. Collectively, these data suggest that RBP4-mediated suppression of PCV2 via selective autophagy is dependent on TLR4 (Supplementary Fig. 6e).

Discussion

The biological functions of RBP4 in health and disease have been extensively studied since its discovery[3]. As a member of the lipocalin family and major transport protein of retinol (also known as vitamin A), it has been established that RBP4 is an adipokine consistently associated with adiposity and insulin resistance in both humans and animal models[34,35]. Although most of RBP4's actions depend on its role in retinoid homeostasis, functions independent of retinol transport have been described[3]. For example, in the immune system, RBP4 expression drives inflammatory responses mediated by TLRs in antigen-presenting cells, such as dendritic cells and macrophages[8]. Moreover, recent studies demonstrate strong correlations between RBP4 levels and infection by multiple viruses[9,11,12]. However, the roles of RBP4 in virus infection are still unclear. Here, we identified RBP4 as a host restriction factor of PCV2 replication, providing an example that RBP4 functions as a key regulator of viral infection without depending on retinol transport. Specifically, secreted RBP4 activates TLR4-mediated selective autophagy to impair the stability of PCV2 ORF1 in a feedback manner. Notably, the protein level of RBP4 was strikingly elevated in multiple cell types in response to PCV2 infection, and such an increase in RBP4 likely serves as a host defensive mechanism. Thus, our data expand the understanding of RBP4 functions in host defense against viral infection.

As the smallest virus known to infect mammals, PCV2 replication relies heavily on the host cells[13]. Although PCV2 replication is not reproductive in macrophages or dendritic cells, PCV2 may alter the function of these cells, thus favoring the survival and spread of the viral particles, which may contribute to viral pathogenesis. In fact, previous studies show that PCV2 regulates innate immune responses and increases host susceptibility to secondary or concurrent viral or bacterial infections[13,15]. Here, we found that PCV2 infection augmented RBP4 expression at the post-transcriptional level via the MAPK–eIF4E signaling pathway. In turn, the host factor RBP4 suppressed PCV2 replication via degradation of ORF1 in a feedback manner. Hence, RBP4 expression limited the productive replication of PCV2 in cells. Notably, a recent study reports that the levels of RBP4 transcripts and protein are increased in the presence of HCV core protein, and knockdown of RBP4 has a positive impact on HCV replication in hepatocytes[9]. By contrast, we found that PCV2 infection did not regulate RBP4 transcription but promoted the protein synthesis of RBP4 to inhibit PCV2 replication. Therefore, cellular circumstances may determine the

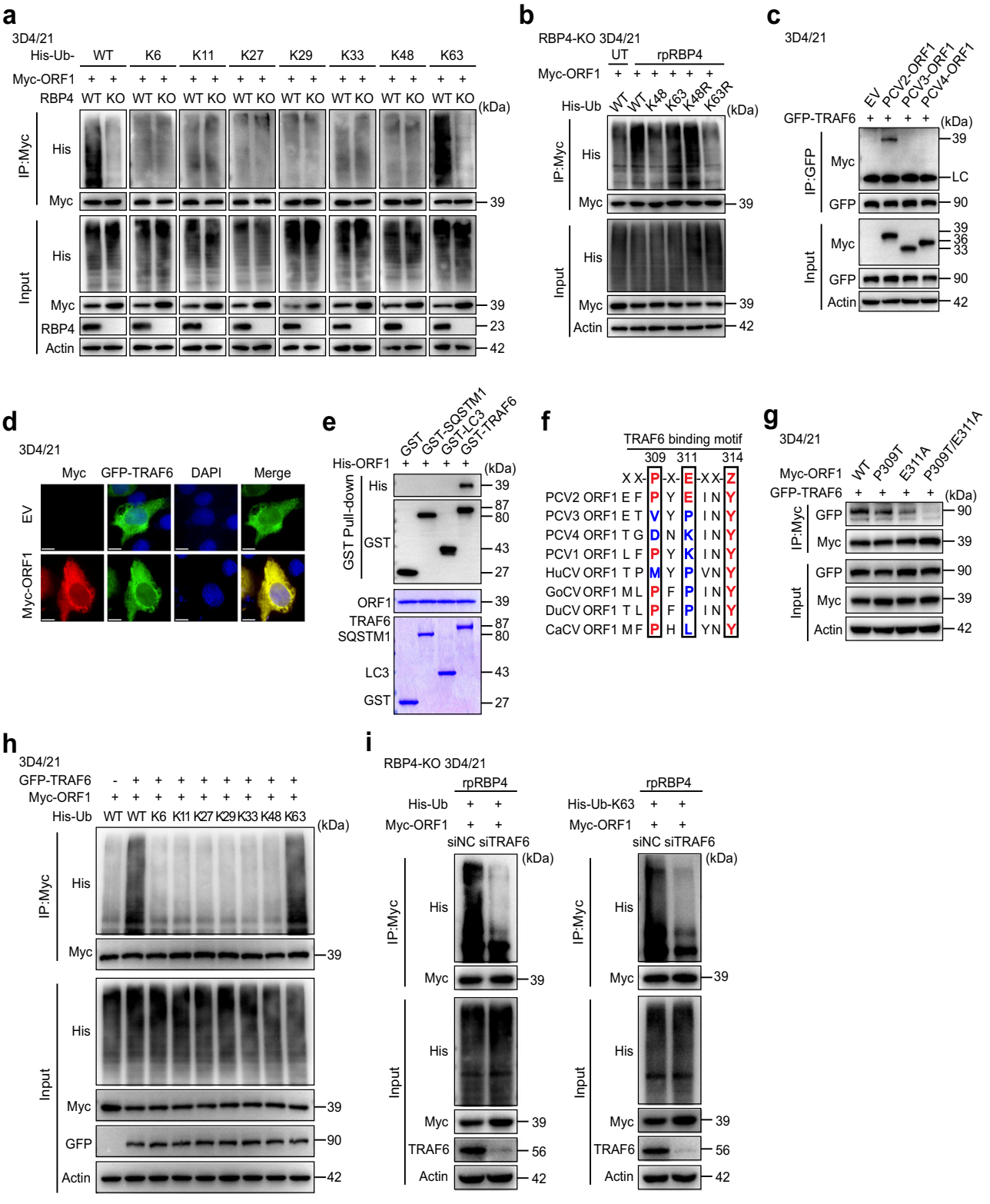

effect of RBP4 on different viruses. Interestingly, macrophages have been identified as major sites of RBP4, and retinoic acid 6 (STRA6), the canonical receptor of RBP4, is not expressed in macrophages[8,27]. Hence, it is reasonable that RBP4 modulates different viruses by distinct mechanisms. Our results thus reveal a previously undescribed antiviral mechanism against PCV2 in infected cells.

Appropriate autophagy is a prerequisite for host defense and immune responses[36]. Specifically, through autophagy receptor engagement, selective autophagy can function as an efficient defense mechanism against various viruses by degradation of viral components or particles[23,37]. Meanwhile, multiple viruses have been shown to induce autophagy to benefit their replication[38,39]. These studies indicate that autophagy plays a dual role in host antiviral responses. Accumulating evidence suggests that PCV2 infection can trigger autophagic processes that favor PCV2 replication in both PK-15 cells and 3D4/21 cells by different mechanisms[40,41]. However, whether and how PCV2 replication is regulated by selective autophagy

Fig. 6 | RBP4 activates TRAF6 to initiate K63-linked polyubiquitination of PCV2 ORF1. a Immunoprecipitation analysis of WT and RBP4-KO 3D4/21 cells transfected with PCV2 ORF1 and His-Ubiquitin (His-Ub) or His-Ub at K6 (His-Ub-K6), K11 (His-Ub-K11), K27 (His-Ub-K27), K29 (His-Ub-K29), K33 (His-Ub-K33), K48 (His-Ub-K48) or K63 (His-Ub-K63) only for 24 h. **b** Immunoprecipitation analysis of RBP4-KO 3D4/21 cells expressing PCV2 ORF1 and His-Ub, His-Ub-K48, His-Ub-K63, His-Ub-K48R, or His-Ub-K63R as indicated. Cells were left untreated or stimulated with rpRBP4 protein for 6 h before harvest. **c** Immunoprecipitation analysis of 3D4/21 cells expressing GFP-TRAF6 together with empty vector (EV), PCV2 ORF1, PCV3 ORF1, or PCV4 ORF1 as indicated. Anti-GFP immunoprecipitates were analyzed by immunoblotting with anti-Myc antibody. Levels of the transfected proteins were analyzed by immunoblotting with anti-Myc and anti-GFP antibodies. **d** Colocalization of exogenous TRAF6 and PCV2 ORF1 in 3D4/21 cells. Cells were transfected with GFP-TRAF6 and PCV2 ORF1 for 24 h before confocal microscopy. Scale bar, 10 μm. **e** GST pull-down analysis of the interaction between His-ORF1 and GST, GST-SQSTM1/p62, GST-LC3, or GST-TRAF6 as indicated. Recombinant proteins were pulled down by GST magnetic beads and were analyzed by immunoblotting with anti-His or anti-GST antibodies (upper). Recombinant proteins in the assay were examined by SDS–PAGE and coomassie blue staining (lower). **f** Schematic drawings of the TRAF6-binding motif Pro-X-Glu-X-X-Ar/Ac. The presence of the putative Pro-X-Glu-X-X-Ar/Ac motifs in ORF1 of PCV2 and other representative circoviruses (PCV3, KX778720.1(Genebank number); PCV4, MK986820.1; PCV1, U49186.1; HuCV2, ON226770.2; GoCV, MT831941.1; DuCV, MN078101.1; and CaCV, JQ821392.1) were analyzed and consistent amino acids are indicated in color. **g** Immunoprecipitation analysis of the association of PCV2 ORF1 and TRAF6 in 3D4/21 cells transfected with GFP-TRAF6 and wild-type PCV2 ORF1 (WT), or PCV2 ORF1 mutants (P309T, E311A, or P309T/E311A). Anti-Myc immunoprecipitates were analyzed by immunoblotting with anti-GFP or anti-Myc antibody as indicated. Levels of the transfected proteins were analyzed by immunoblotting with anti-GFP or anti-Myc antibody. **h** Immunoprecipitation analysis of 3D4/21 cells expressing PCV2 ORF1 and His-Ub, His-Ub-K6, His-Ub-K11, His-Ub-K27, His-Ub-K29, His-Ub-K33, His-Ub-K48 or His-Ub-K63 together with or without GFP-TRAF6 as indicated. **i** Immunoblotting analysis of the indicated proteins in immunoprecipitated samples and whole-cell lysates of RBP4-KO 3D4/21 cells transfected with TRFA6 siRNA or control siRNA (100 nM). Twenty-four hours after transfection, cells were further transfected with PCV2 ORF1 and His-Ub (left) or His-Ub-K63 (right) for 24 h. Cells were then stimulated with rpRBP4 (30 μg/mL) for 6 h before analysis. Data are representative of three (**c**–**g**) or two (**a**, **b**, **h**, **i**) independent experiments.

remain unclear. Herein, we demonstrated that RBP4 initiates selective autophagy through TRAF6 and SQSTM1/p62, which facilitates the recruitment of ubiquitin-tagged ORF1 protein into autophagosomes for degradation. To the best of our knowledge, this is the first report that selective autophagy plays a critical role in the modulation of PCV2 infection.

Having a ubiquitin-binding domain, the autophagy receptor SQSTM1/p62 is reported to recruit K63-linked ubiquitin-conjugated substrates to autophagosomes, which is catalyzed by the E3 ligase TRAF6[42]. Interestingly, we found that RBP4 triggered SQSTM1/p62-mediated selective autophagy through activation of TLR4 signaling. Because TRAF6 is the downstream kinase of the TLR4 signaling pathway, it is not surprising that RBP4 promotes activation of the E3 ligase TRAF6 to mediate K63-linked ubiquitination of PCV2 ORF1. In fact, we identified five critical residues (K15, K66, K67, K94, and K99) of PCV2 ORF1 that are targeted for K63-linked polyubiquitination by TRAF6. Hence, our results identified a previously unappreciated mechanism for TRAF6 in the regulation of selective autophagy and viral protein ubiquitination.

Circoviruses belong to the Ciroviridae family, which contains viruses with circular, single-stranded DNA genomes and a wide range of hosts. Among them, PCV is the smallest of the Ciroviridae, and four PCV species (PCV1–PCV4) have been described. Although there is no direct evidence of zoonotic transmission of PCVs from animals to humans, several studies report the detection of PCV in human samples or nonhuman primates[43,44]. More recently, a novel circovirus in humans named HuCV2 that is closely to PCV3 has been identified, raising concerns about its origin, prevalence, and pathogenicity in humans[45]. Therefore, effective control of PCV infection is important for the health of both humans and animals. Despite the availability of effective vaccines for PCVD, they are currently not therapeutic. The virus re-emerges shortly after vaccination is suspended and is difficult to eradicate[46]. One critical characteristic of PCV2 replication in cell culture is that it typically yields very low viral titers, which has restricted the production of vaccines[47]. It seems that this low reproductive rate of some circoviruses is a common feature due to their deep interaction with the host cells. Here, we demonstrate that RBP4 is a key suppressor for PCV2 productive replication through targeting ORF1 degradation. Importantly, the ORF1 or *rep* gene encodes for proteins associated with replication for circoviruses. Given that PCV2, PCV3, and HuCV2 have similar structures, it is possible that key host factors may exist to regulate productive replication of all circoviruses. Our current findings provide a good example of how a host restriction factor play pivotal roles in the regulation of circovirus replication and identifies a critical mechanism for crosstalk between circovirus and host cells.

In summary, we demonstrated that PCV2 infection activates the MAPK–eIF4E axis to induce RBP4 protein expression. Subsequently, RBP4 functions as a suppressor of PCV2 replication via launching TRAF6 and SQSTM1/p62-mediated selective autophagy to impair the stability of the ORF1 replicase. Hence, our results identify a key function of RBP4 in regulation of virus infection, which restricts PCV2 productive replication in macrophages.

Methods

Ethics statement

All animal protocols were reviewed and approved by the Shandong Agricultural University Animal Care and Use Committee (Approval Number: # SDAUA-2018-057) and were performed according to the Animal Ethics Procedures and Guidelines of the People's Republic of China. We have complied with all relevant ethical regulations for animal use.

Cells and cell culture

HeLa, 3D4/21, and PK-15 cells were from the American Type Culture Collection (ATCC, VA, USA). RBP4-deficient HeLa cells, RBP4-deficient 3D4/21 cells, and RBP4-deficient PK-15 cells were generated by CRISPR-Cas9 editing. Cells were maintained in Dulbecco's modified Eagle's medium (DMEM) containing 10% fetal bovine serum (FBS) (Biological Industries, Israel) and 1% penicillin–streptomycin (Gibco) at 37 °C and 5% CO_2. Murine bone marrow-derived macrophages (BMDMs) were obtained and cultured as previously described[26]. Porcine alveolar macrophages (PAMs) obtained by bronchoalveolar lavages from the lungs of two specific pathogen-free piglets as previously described[48]. All cells tested negative for mycoplasma.

Mice

C57BL/6 mice were purchased from Beijing Vital River Laboratory Animal Technology Co., Ltd. RBP4-deficient mice in the C57BL/6 genetic background were obtained from the Center for Animal Resources and Development, Kumamoto University (Honjo, Kumamoto, Japan)[2]. All mice were maintained in pathogen-free barrier facilities. Mice genotypes were identified by PCR assays with specific primers (GSP-F: CTCGGCTCCGTC GCTCCACG, GSP-R: CCAGAGCCCAGAGAACTGAG, and mPGK-R: TACCCGCTTCCATTGCTCAG). Female littermates with the $Rbp4^{+/+}$ and $Rbp4^{-/-}$ genotypes at 6–8 weeks of age were used for all experiments.

Virus infection

The PCV2b strain (strain IDSDTA2017-1) was previously isolated and identified[15]. For PCV2 infection in vitro, cells were infected with PCV2b (MOI = 0.2) for various times or were infected with the indicated doses of PCV2b for 36 h before further analysis. For in vivo infection, mice were

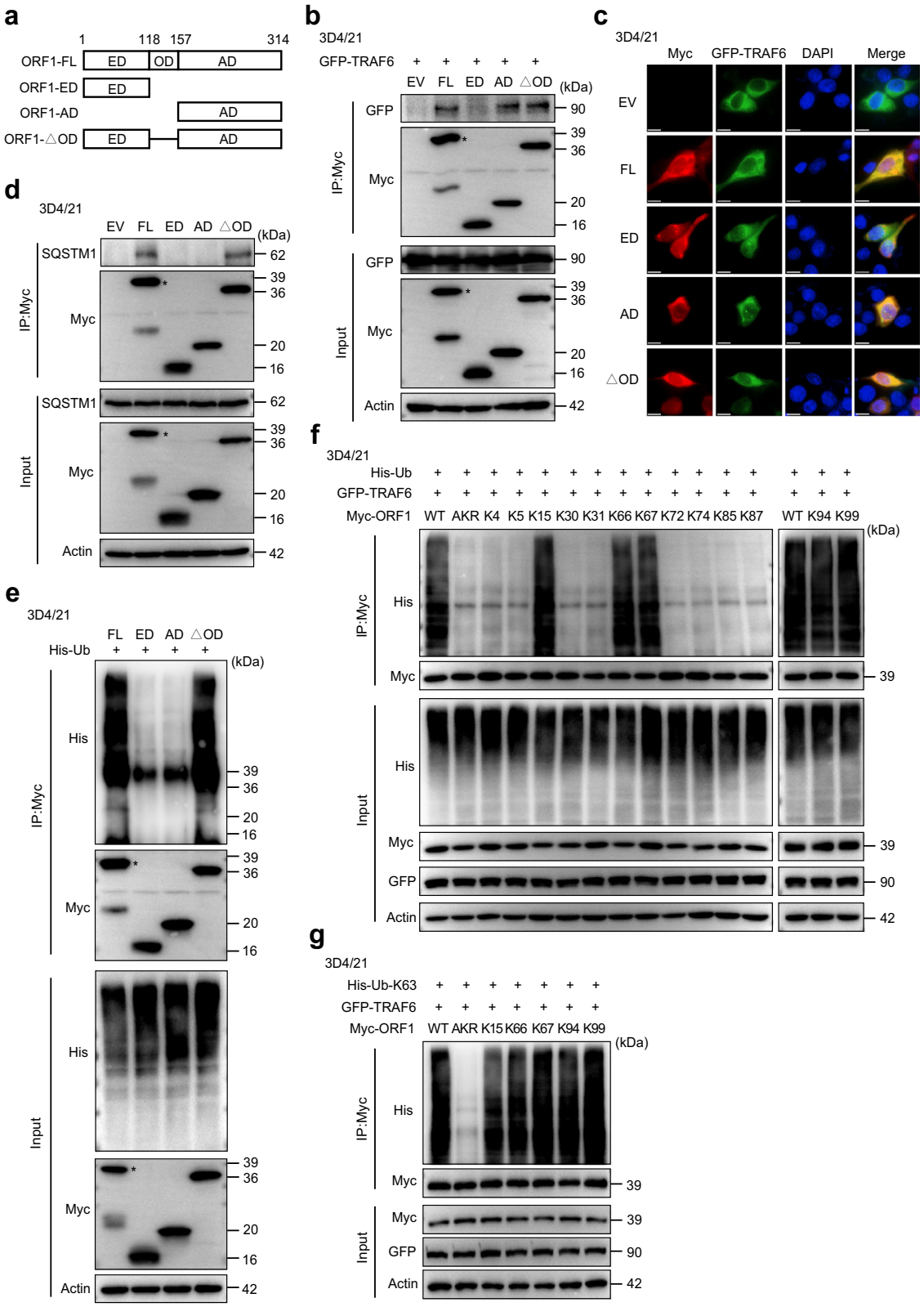

intraperitoneally injected with PCV2b (5×10^5 pfu/mouse) for 7 days before further analysis.

Antibodies and reagents

The antibodies used and their sources are as follows: anti-PCV2 Cap polyclonal antibody was previously generated[49]. Antibodies against phospho-p38 (9215, 1:1000), anti-Erk1/2 (9102, 1:1000), anti-p-Erk1/2 (9101, 1:1000), anti-p-p65 (3033, 1:1000), anti-JNK (9252, 1:1000), anti-p-JNK (9255, 1:1000), anti-eIF4E (2067, 1:1000), and anti-p-eIF4E (9741, 1:1000) were obtained from Cell Signaling Technology. Anti-RBP4 (66104-1, 1:3000), anti-TRAF6 (66498-1, 1:1000), anti-p65 (10745-1-AP, 1:1000), anti-HA tag (51064-2-AP, 1:5000), anti-His tag (10001-0-AP, 1:5000), anti-

Fig. 7 | TRAF6 interacts with the ATPase domains of PCV2 ORF1 to modulate its ubiquitination and degradation. a Schematic of PCV2 ORF1 domains and mutants. ED (amino acids 1–118) indicates the N-terminal endonuclease domain, OD (amino acids 119–157) indicates the oligomerization domain, and AD (amino acids 158–314) is the C-terminal ATPase domain. The ORF1-ΔOD mutant was generated by deletion of the OD domain. **b** Immunoblotting analysis of TRAF6 and PCV2 ORF1 in immunoprecipitated samples or whole-cell lysates of 3D4/21 cells transfected with GFP-pTRAF6 and empty vector, full-length PCV2 ORF1 Myc-ORF1-FL (FL), or truncated PCV2 ORF1 Myc-ORF1-ED (ED), Myc-ORF1-AD (AD), or Myc-ORF1-ΔOD (ΔOD). Anti-Myc immunoprecipitates were analyzed by immunoblotting with anti-GFP or anti-Myc antibody as indicated. Levels of the transfected proteins were analyzed by immunoblotting with anti-GFP or anti-Myc antibody. **c** Colocalization of TRAF6 and full-length PCV2 ORF1 or truncated ORF1. 3D4/21 cells were transfected with GFP-pTRAF6 and full-length or truncated PCV2 ORF1 plasmids for 24 h before confocal microscopy. Scale bar, 10 μm. **d** Immunoblotting analysis of SQSTM1 and PCV2 ORF1 in immunoprecipitated samples or whole-cell lysates of 3D4/21 cells transfected with empty vector, full-length or truncated PCV2 ORF1. Anti-Myc immunoprecipitates were analyzed by immunoblotting with an anti-SQSTM1 antibody or anti-Myc antibody as indicated. Levels of the transfected proteins were analyzed by immunoblotting with an anti-Myc or anti-SQSTM1 antibody. **e** Immunoprecipitation analysis of 3D4/21 cells expressing His-Ub with full-length or truncated PCV2 ORF1. Anti-Myc immunoprecipitates were analyzed by immunoblotting with an anti-His or anti-Myc antibody. Levels of the transfected proteins were analyzed by immunoblotting with anti-Myc antibody as indicated. **f** Immunoprecipitation analysis of 3D4/21 cells expressing His-Ub, GFP-pTRAF6 together with wild-type (WT) PCV2 ORF1 or ORF1 mutants (K4, K5, K15, K30, K31, K66, K67, K72, K74, K85, K87, K94, and K99 only; or Lys-to-Arg mutants of all lysines in ORF1 ED domain, AKR) as indicated. Anti-Myc immunoprecipitates were analyzed by immunoblotting with an anti-His or anti-Myc antibody. Levels of the transfected proteins were analyzed by immunoblotting with anti-Myc or anti-GFP antibody as indicated. **g** Immunoprecipitation analysis of 3D4/21 cells expressing His-Ub-K63, GFP-pTRAF6 together with WT PCV2 ORF1-ED or ORF1-ED mutants (K15, K66, K67, K94, K99 only or AKR) as indicated. Anti-Myc immunoprecipitates were analyzed by immunoblotting with an anti-His or anti-Myc antibody. Levels of the transfected proteins were analyzed by immunoblotting with anti-Myc or anti-GFP antibody as indicated. Data are representative of three (**b**–**d**) or two (**e**–**g**) independent experiments.

GFP tag (50430-2-AP, 1:2000), and anti-β-actin (66009-1-lg, 1:20,000) were from Proteintech Group, Inc. anti-GST tag (AF2888, 1:2000) was purchased from Beyotime Biotechnology. Anti-Flag antibody (F1804; 1:1000) and anti-LC3B antibody (L7543; 1:1000) were purchased from Sigma-Aldrich. Antibodies against-c-Myc (9E10; 1:1000) and anti-p38 antibody (sc-7972; 1:1000) were from Santa Cruz Biotechnology. Lipopolysaccharides (LPS, from *Escherichia coli* O111:B4) was from Sigma-Aldrich. Poly(I:C) and Poly(dA:dT) were from Invivogen. Chemical inhibitors BAY11-7082 (HY-13453), U0126 (HY-12031A), SB203580 (HY-10256), SP600125 (HY-12041), MG132 (HY-13259), Cycloheximide (HY-12320), Rapamycin (HY-10219), and Chloroquine (HY-17589A) were from MedChemExpress. Recombinant human RBP4 (rhRBP4, 3378-LC) was obtained from R&D Systems. Recombinant porcine RBP4 was previously generated[50]. Lipofectamine 2000 was purchased from Thermo Fisher Scientific.

Plasmids

Porcine RBP4 was amplified by PrimeSTAR HS DNA Polymerase (Takara Bio, Beijing, China) with cDNA of 3D4/21 cells as a template, followed by *Hind* III and *Kpn* I digestion, and was ligated into the pcDNA3.0-Flag vector (Addgene). Porcine TRAF6, SQSTM1/p62, NBR1, CALCOCO2/NDP52, OPTN, TOLLIP, and TAX1BP1 were amplified from the cDNA of 3D4/21 cells and were cloned into the pEGFP-C1 vector, respectively. Human TRAF6 (hTRAF6) was amplified from cDNA of HeLa cells and was ligated with pEGFP-C1 vector. PCV2b-ORF1 and its truncation mutants (amino acids 1–118, amino acids 158–314, and amino acids Δ119–157), ORF2, ORF3, ORF4, and ORF5 were amplified from PCV2b (strain IDSDTA2017-1) genomic DNA and cloned into the pCMV-Myc vector (Addgene). Ubiquitin mutants (K6, K11, K27, K29, K33, K48, K63, K48R, and K63R) were previously generated[51]. PCV2-ORF1 mutants (P309T, E311A, and P309T/E311A) or ORF1 lysine mutants (K4, K5, K15, K30, K31, K66, K67, K72, K74, K85, K87, K94, K99, and AKR) were generated by using a Site-Directed Mutagenesis Kit according to the manufacturer's protocol (New England Biolabs, USA). pEGFP-LC3B was provided by Dr. Yushan Zhu (Nankai University, China). The pCMV-Myc-PCV3-ORF1 and pCMV-Myc-PCV4-ORF1 vectors were synthesized and constructed by GENEWIZ, Inc. The PCV3 ORF1 sequence was derived from PCV3 (strain PCV3-US/MO2015, GenBank: KX778720.1), and the PCV4 ORF1 sequence was derived from PCV4 (strain HNU-AHG1-2019, GenBank: MK986820.1). Porcine SQSTM1/p62, LC3, and TRAF6 were amplified from the cDNA of 3D4/21 cells and were cloned into the pGEX-6P-1 vector, respectively. PCV2b-ORF1 was amplified from PCV2b genomic DNA and cloned into the pET-30a vector. The primers used to construct these expression vectors are listed in Supplementary Table 1. All constructs followed standard molecular cloning protocols and were then sequenced. Protein expression of the constructs was further confirmed by immunoblotting.

DNA quantification

Total viral DNA was extracted using a DNA isolation kit (TIANGEN, China) following the manufacturer's protocol. PCV2 DNA copies were quantified by qPCR using the ORF2 gene primers that are listed in Supplementary Table 1. Viral growth kinetics assays were performed as previously described[52].

Reverse transcription and quantitative real-time PCR (qPCR)

Total RNA was extracted using an Eastep Super Total RNA Extraction Kit (Promega) and was reverse transcribed into cDNA using M-MLV reverse transcriptase with RNase inhibitor (Takara Bio, Beijing, China). qPCR was performed in triplicate experiments with RealStar Green Fast Mixture (A303, GenStar) on a StepOne plus thermal cycler (ABI, Thermo Fisher Scientific). Threshold cycle numbers were normalized to triplicate samples amplified with primers specific for glyceraldehyde-3-phosphate dehydrogenase (*GAPDH*). All qPCR primer sequences are listed in Supplementary Table 1.

RNA interference

Small interfering RNAs (siRNA) specifically targeting human SQSTM1/p62, NBR1, NDP52, and OPTN and a non-targeting control siRNA were previously reported[53–56]. Porcine TRAF6 siRNA oligos were designed by Shanghai GenePharma Co., Ltd., China. All siRNA oligos were synthesized by Shanghai GenePharma Co., Ltd., China, and were transfected into HeLa cells or 3D4/21 cells using Lipofectamine RNAiMAX reagent (Thermo Fisher Scientific, USA) according to the manufacturer's instructions at a final concentration of 100 nM. The porcine TRAF6 siRNA target sequences are listed as follows: siTRAF6#1 (porcine): 5′-GCAGAUGGGGCAUUCAUATT-3′; and siTRAF6#2 (porcine): 5′-UAUGAAUGCCCCAUCUGCTT-3′.

Generation of RBP4 knockout cells

To generate RBP4 knockout cells, custom gRNAs targeting the human *RBP4* gene and porcine *RBP4* gene were designed using the gRNA website (http://crispr.mit.edu) and were synthesized (Sango Biotech, Shanghai, China). The human gRNA sequences were ligated to PX459M plasmid and EZ-Guide-XH, respectively, and were then digested by *Xho* I and *Hind* III enzymes. Finally, the two gRNAs were ligated into PX459M plasmids to generate PX459M-EZ-hRBP4-gRNA1/2 plasmid containing two different gRNAs. The porcine gRNA sequences were ligated into the PX459M plasmid to generate the PX459M-pRBP4-gRNA plasmid. HeLa cells, 3D4/21 cells, or PK-15 cells were transfected with PX459M-EZ-hRBP4-gRNA1/2 or PX459M-pRBP4-gRNA and control vector. At 24 h after transfection, cells were screened with puromycin (3 μg/mL, Solarbio, China) for 7 days. Monoclonal cells were obtained by the limited dilution method in 96-well

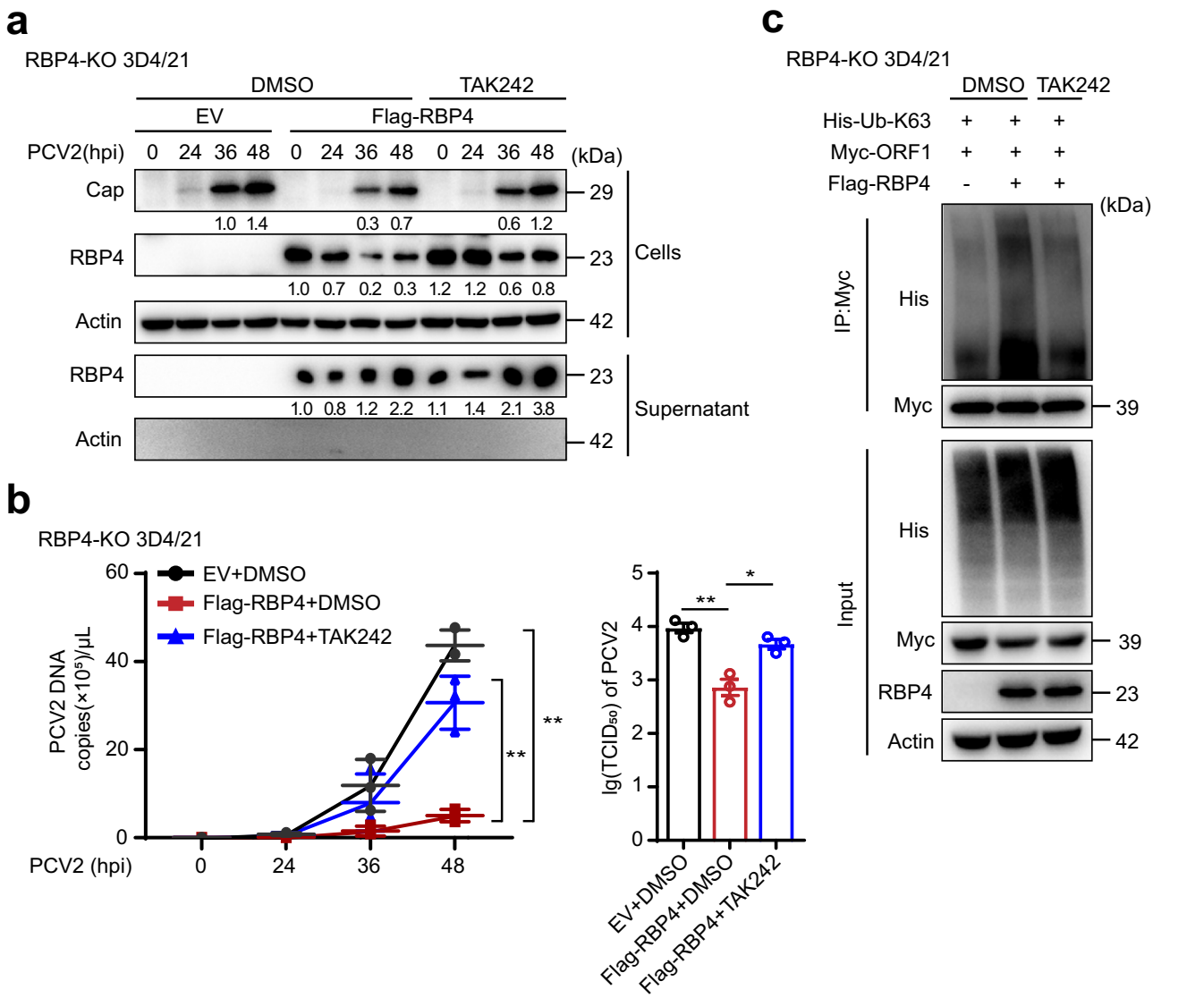

Fig. 8 | RBP4 binds TLR4 to activate TRAF6-mediated ubiquitination of PCV2 ORF1 in macrophages. Immunoblotting analysis of PCV2 Cap protein level (**a**) or qPCR analysis of PCV2 DNA copies (**b**, left) or TCID50 assay of viral titers (**b**, right) in RBP4-KO 3D4/21 cells transfected with empty vector (EV) or Flag-pRBP4 plasmid for 6 h, then cells were treated for 6 h with or without TLR4-specific inhibitor TAK242 (1 μM), followed by infection with PCV2 for the indicated periods or 48 h. Numbers (lower) indicate the grayscale analysis on the protein bands of Cap and RBP4. **c** Immunoprecipitation analysis of RBP4-KO 3D4/21 cells expressing PCV2 ORF1 and His-Ub-K63 together with or without Flag-RBP4 as indicated for 6 h. Cells were untreated or treated with TAK242 (1 μM) for 18 h before harvest. Data are representative of three independent experiments (**a**, **c**) or pooled from three independent experiments (**b**, mean ± SD). $^{*}p < 0.05$, $^{**}p < 0.01$ (Student's *t* test).

format, and deficiency of RBP4 was verified by regular PCR following DNA sequencing and immunoblotting.

Co-immunoprecipitation (Co-IP) and immunoblotting

Immunoprecipitation and immunoblotting were performed as previously described[57]. Briefly, cells were transfected with the indicated plasmids using Lipofectamine 2000 (Thermo Fisher Scientific). Twenty-four hours after transfection, cells were lysed on ice with a lysis buffer (50 mM Tris-HCl at pH 7.4, 150 mM NaCl, 1% Triton X-100, 1% sodium deoxycholate, 1 mM Na_3VO_4, 1 mM EDTA, and 1 mM PMSF) for 1 h. After centrifugation for 10 min at 13,000 × *g* and 4 °C, supernatants were collected and incubated with protein A/G PLUS-Agarose beads (sc-2003; Santa Cruz Biotechnology) coupled to 1 μg specific antibodies overnight with rotation at 4 °C. Immunoprecipitated extracts or whole-cell lysates were then separated by SDS–PAGE and transferred to a polyvinylidene fluoride (PVDF) membrane (Millipore) for immunoblotting with specific antibodies.

Immunofluorescence

Immunofluorescence assays were performed as previously described[51]. Briefly, cells were fixed for 20 min in 4% paraformaldehyde, permeabilized with 0.1% Triton X-100 for 10 min, and then blocked with 5% bovine serum albumin (BSA, Sigma) for 30 min. Cells were incubated with the appropriate primary antibodies for 3 h and then stained with Alexa Fluor 594-, 488-, or 637-conjugated secondary antibodies (Proteintech Group Inc., China) for 90 min. Nuclei were stained with DAPI (C1006, Beyotime, China). Images were acquired using a laser scanning confocal microscope with LAS X software (Leica, Germany).

Virus titrations

Virus titers were determined by a microtitration infectivity assay and recorded as $TCID_{50}$/mL by using the Reed–Muench method[58]. In brief, cell suspension was prepared by freeze–thawed method for three times. Tissues were homogenized in DMEM to make 10% (weight/volume) tissue

homogenates. Cell suspension or tissue homogenates were then clarified by centrifugation and titrated in 96-well tissue culture plates containing PK-15 cell monolayers for immunofluorescence assay with anti-Cap antibody for $TCID_{50}$ calculation.

GST pull-down assay

GST pull-down assays were performed as previously described[59]. Briefly, GST- or His-tagged recombinant proteins were expressed in *Escherichia coli* (BL21) at 16 °C for 12 h. Recombinant proteins were purified with GSTrap FF columns or HisTrap HP according to the manufacturer's protocol (GE Healthcare, USA). For pull-down assay, equal amounts (25 μg) of purified recombinant proteins (GST, GST-SQSTM1, GST-LC3, or GST-TRAF6) were firstly incubated with His-ORF1 for overnight with rotation at 4 °C, respectively. After that, GST magnetic beads (Beaver Biosciences, China) were added for incubation for another 4 h. The bound proteins were then examined by SDS–PAGE and Coomassie brilliant blue staining or immunoblotting.

Histopathology

Wild-type and Rbp4-deficient mice were euthanized at 7 days post PCV2 challenge, and lung or liver tissues from sacrificed animals were obtained. Tissues were cut into appropriate tissue blocks and fixed in 10% neutral-buffered formalin for 24 h. After dehydration and embedding in paraffin, tissue samples were cut into 3 μm thick sections, mounted onto glass slides, and stained with hematoxylin and eosin (H&E) as previously described[51]. Images were acquired on an Olympus microscope (CX41RF) using imaging software (MiE V3.1). Histological scores were evaluated as previously described[60,61].

Statistics and reproducibility

GraphPad Prism 9.0 software (Chicago, IL, USA) was used to perform statistical analysis, and the unpaired Student's *t* test (two-tailed) was used to determine significant differences. The P value < 0.05 or P value < 0.01 was considered as the statistical significance. All data are shown as mean value ± standard deviation (SD). Information about the number of experimental replicates, sample sizes, statistical analyses, and P values can be found in the figure legends. The data of western blots were acquired from at least two independent biological replicates, and other data were acquired from three independent biological replicates.

Reporting summary

Further information on research design is available in the Nature Portfolio Reporting Summary linked to this article.

Data availability

All data are available in the main text or the Supplementary Materials. The numerical source data behind the graphs in the paper can be found in Supplementary Data. Unprocessed blot images can be found in Supplementary Fig. 7.

Received: 18 March 2024; Accepted: 11 October 2024;
Published online: 05 November 2024

References

1. Ji, Y., Song, J., Su, T. & Gu, X. Adipokine retinol binding protein 4 and cardiovascular diseases. *Front. Physiol.* **13**, 856298–856298 (2022).
2. Shen, J. et al. Severe ocular phenotypes in Rbp4-deficient mice in the C57BL/6 genetic background. *Lab. Investig.* **96**, 680–691 (2016).
3. Steinhoff, J. S., Lass, A. & Schupp, M. Biological functions of RBP4 and its relevance for human diseases. *Front. Physiol.* **12**, 659977 (2021).
4. Kawaguchi, R. et al. A membrane receptor for retinol binding protein mediates cellular uptake of vitamin A. *Science* **315**, 820–825 (2007).
5. Yang, Q. et al. Serum retinol binding protein 4 contributes to insulin resistance in obesity and type 2 diabetes. *Nature* **436**, 356–362 (2005).
6. Broch, M. et al. Macrophages are novel sites of expression and regulation of retinol binding protein-4 (RBP4). *Physiol. Res.* **59**, 299–303 (2010).
7. Moraes-Vieira, P. M. et al. Retinol binding protein 4 primes the NLRP3 inflammasome by signaling through toll-like receptors 2 and 4. *Proc. Natl. Acad. Sci. USA* **117**, 31309–31318 (2020).
8. Moraes-Vieira, P. M. et al. RBP4 activates antigen-presenting cells, leading to adipose tissue inflammation and systemic insulin resistance. *Cell Metab.* **19**, 512–526 (2014).
9. Gouthamchandra, K. et al. Serum proteomics of hepatitis C virus infection reveals retinol-binding protein 4 as a novel regulator. *J. Gen. Virol.* **95**, 1654–1667 (2014).
10. Wen, L. et al. Comparative proteomic profiling and biomarker identification of traditional Chinese medicine-based HIV/AIDS syndromes. *Sci. Rep.* **8**, 4187 (2018).
11. Fu, Y. et al. Protein profiling of nasopharyngeal aspirates of hospitalized and outpatients revealed cytokines associated with severe influenza A (H1N1) pdm09 virus infections: a pilot study. *Cytokine* **86**, 10–14 (2016).
12. Wysocki, M. et al. Identifying putative candidate genes and pathways involved in immune responses to porcine reproductive and respiratory syndrome virus (PRRSV) infection. *Anim. Genet.* **43**, 328–332 (2012).
13. Meng, X. J. Porcine circovirus type 2 (PCV2): pathogenesis and interaction with the immune system. *Annu. Rev. Anim. Biosci.* **1**, 43–64 (2013).
14. Trible, B. R. & Rowland, R. R. Genetic variation of porcine circovirus type 2 (PCV2) and its relevance to vaccination, pathogenesis and diagnosis. *Virus Res.* **164**, 68–77 (2012).
15. Zhang, W. et al. Macrophage polarization modulated by porcine circovirus type 2 facilitates bacterial coinfection. *Front. Immunol.* **12**, 688294 (2021).
16. Ramamoorthy, S. & Meng, X. J. Porcine circoviruses: a minuscule yet mammoth paradox. *Anim. Health Res. Rev.* **10**, 1–20 (2009).
17. Choi, Y., Bowman, J. W. & Jung, J. U. Autophagy during viral infection - a double-edged sword. *Nat. Rev. Microbiol.* **16**, 341–354 (2018).
18. Vargas, J. N. S., Hamasaki, M., Kawabata, T., Youle, R. J. & Yoshimori, T. The mechanisms and roles of selective autophagy in mammals. *Nat. Rev. Mol. Cell Biol.* **24**, 167–185 (2023).
19. Khaminets, A., Behl, C. & Dikic, I. Ubiquitin-dependent and independent signals in selective autophagy. *Trends Cell Biol.* **26**, 6–16 (2016).
20. Shaid, S., Brandts, C. H., Serve, H. & Dikic, I. Ubiquitination and selective autophagy. *Cell Death Differ.* **20**, 21–30 (2013).
21. Judith, D. et al. Species-specific impact of the autophagy machinery on Chikungunya virus infection. *EMBO Rep.* **14**, 534–544 (2013).
22. Berryman, S. et al. Foot-and-mouth disease virus induces autophagosomes during cell entry via a class III phosphatidylinositol 3-kinase-independent pathway. *J. Virol.* **86**, 12940–12953 (2012).
23. Kong, N. et al. BST2 suppresses porcine epidemic diarrhea virus replication by targeting and degrading virus nucleocapsid protein with selective autophagy. *Autophagy* **16**, 1737–1752 (2020).
24. Ma, Z. et al. Tegument protein UL21 of alpha-herpesvirus inhibits the innate immunity by triggering CGAS degradation through TOLLIP-mediated selective autophagy. *Autophagy* **19**, 1512–1532 (2023).
25. Deng, T. et al. TRAF6 autophagic degradation by avibirnavirus VP3 inhibits antiviral innate immunity via blocking NFKB/NF-κB activation. *Autophagy.* **18**, 2781–2798 (2022).
26. Xu, H. et al. Notch-RBP-J signaling regulates the transcription factor IRF8 to promote inflammatory macrophage polarization. *Nat. Immunol.* **13**, 642–650 (2012).
27. Norseen, J. et al. Retinol-binding protein 4 inhibits insulin signaling in adipocytes by inducing proinflammatory cytokines in macrophages through a c-Jun N-terminal kinase- and toll-like receptor 4-dependent and retinol-independent mechanism. *Mol. Cell. Biol.* **32**, 2010–2019 (2012).

28. Ciechanover, A. Proteolysis: from the lysosome to ubiquitin and the proteasome. *Nat. Rev. Mol. Cell Biol.* **6**, 79–87 (2005).
29. Gatica, D., Lahiri, V. & Klionsky, D. J. Cargo recognition and degradation by selective autophagy. *Nat. Cell Biol.* **20**, 233–242 (2018).
30. Pohl, C. & Dikic, I. Cellular quality control by the ubiquitin-proteasome system and autophagy. *Science* **366**, 818–822 (2019).
31. Shi, C. S. & Kehrl, J. H. TRAF6 and A20 regulate lysine 63-linked ubiquitination of Beclin-1 to control TLR4-induced autophagy. *Sci. Signal.* **3**, ra42 (2010).
32. Ye, H. et al. Distinct molecular mechanism for initiating TRAF6 signalling. *Nature* **418**, 443–447 (2002).
33. Tarasova, E., Dhindwal, S., Popp, M., Hussain, S. & Khayat, R. Mechanism of DNA interaction and translocation by the replicase of a circular Rep-encoding single-stranded DNA virus. *mBio* **12**, e0076321 (2021).
34. Yao, J. M. et al. Exosomal RBP4 potentiated hepatic lipid accumulation and inflammation in high-fat-diet-fed mice by promoting M1 polarization of Kupffer cells. *Free Radic. Biol. Med.* **195**, 58–73 (2023).
35. Olsen, T. & Blomhoff, R. Retinol, retinoic acid, and retinol-binding protein 4 are differentially associated with cardiovascular disease, type 2 diabetes, and obesity: an overview of human studies. *Adv. Nutr.* **11**, 644–666 (2020).
36. Deretic, V., Saitoh, T. & Akira, S. Autophagy in infection, inflammation and immunity. *Nat. Rev. Immunol.* **13**, 722–737 (2013).
37. Viret, C., Duclaux-Loras, R., Nancey, S., Rozières, A. & Faure, M. Selective autophagy receptors in antiviral defense. *Trends Microbiol.* **29**, 798–810 (2021).
38. Zhao, S. et al. Genome-scale CRISPR-Cas9 screen reveals novel regulators of B7-H3 in tumor cells. *J. Immunother. Cancer* **10**, e004875 (2022).
39. Sun, M. X. et al. Porcine reproductive and respiratory syndrome virus induces autophagy to promote virus replication. *Autophagy* **8**, 1434–1447 (2012).
40. Wang, X. et al. MicroRNA-30a-5p promotes replication of porcine circovirus type 2 through enhancing autophagy by targeting 14-3-3. *Arch. Virol.* **162**, 2643–2654 (2017).
41. Lv, J. et al. Porcine circovirus type 2 ORF5 protein induces autophagy to promote viral replication via the PERK-eIF2α-ATF4 and mTOR-ERK1/2-AMPK signaling pathways in PK-15 cells. *Front. Microbiol.* **11**, 320–334 (2020).
42. Seibenhener, M. L. et al. Sequestosome 1/p62 is a polyubiquitin chain binding protein involved in ubiquitin proteasome degradation. *Mol. Cell. Biol.* **24**, 8055–8068 (2004).
43. Krüger, L. et al. Transmission of porcine circovirus 3 (PCV3) by xenotransplantation of pig hearts into baboons. *Viruses* **11**, 650–661 (2019).
44. Tischer, I. et al. Presence of antibodies reacting with porcine circovirus in sera of humans, mice, and cattle. *Arch. Virol.* **140**, 1427–1439 (1995).
45. Li, Y. et al. Novel circovirus in blood from intravenous drug users, Yunnan, China. *Emerg. Infect. Dis.* **29**, 1015–1019 (2023).
46. Afghah, Z., Webb, B., Meng, X. J. & Ramamoorthy, S. Ten years of PCV2 vaccines and vaccination: Is eradication a possibility? *Vet. Microbiol.* **206**, 21–28 (2017).
47. Yang, X. et al. Comparative analysis of different methods to enhance porcine circovirus 2 replication. *J. Virol. Methods* **187**, 368–371 (2013).
48. Han, J., Zhang, S., Zhang, Y., Chen, M. & Lv, Y. Porcine circovirus type 2 increases interleukin-1beta and interleukin-10 production via the MyD88-NF-kappa B signaling pathway in porcine alveolar macrophages in vitro. *J. Vet. Sci.* **18**, 183–191 (2017).
49. Zhang, W., Liu, Z. Z., Li, J. S. & Shang, Y. L. Preparation and potential application of high-titer polyclonal antibody against capsid protein of porcine circovirus type II. *Biotechnol. Bull.* **36**, 72–79 (2020).
50. Zhao, H. J., Han, Q. B. & Shang, Y. L. Soluble expression purification and biological activity identification of recombinant porcine retinobl binding protein 4. *Chin. J. Vet. Sci.* **43**, 48–56 (2023).
51. Kong, Z. J. et al. Pseudorabies virus tegument protein UL13 recruits RNF5 to inhibit STING-mediated antiviral immunity. *PLoS Pathog.* **18**, e1010544 (2022).
52. Chang, G. N., Hwang, J. F., Chen, J. T., Tsen, H. Y. & Wang, J. J. Fast diagnosis and quantification for porcine circovirus type 2 (PCV-2) using real-time polymerase chain reaction. *J. Microbiol. Immunol. Infect.* **43**, 85–92 (2010).
53. Li, D. et al. p62 overexpression promotes bone metastasis of lung adenocarcinoma out of LC3-dependent autophagy. *Front. Oncol.* **11**, 609548 (2021).
54. Yamamoto, K. et al. Autophagy promotes immune evasion of pancreatic cancer by degrading MHC-I. *Nature* **581**, 100–105 (2020).
55. Thurston, T. L., Ryzhakov, G., Bloor, S., von Muhlinen, N. & Randow, F. The TBK1 adaptor and autophagy receptor NDP52 restricts the proliferation of ubiquitin-coated bacteria. *Nat. Immunol.* **10**, 1215–1221 (2009).
56. Ali, D. M., Ansari, S. S., Zepp, M., Knapp-Mohammady, M. & Berger, M. R. Optineurin downregulation induces endoplasmic reticulum stress, chaperone-mediated autophagy, and apoptosis in pancreatic cancer cells. *Cell Death Discov.* **5**, 128–143 (2019).
57. Ning, F. et al. Hes1 attenuates type I IFN responses via VEGF-C and WDFY1. *J. Exp. Med.* **216**, 1396–1410 (2019).
58. Hu, Y. et al. Truncated Rep protein of porcine circovirus 2 (PCV2) caused by a naturally occurring mutation reduced virus replication in PK15 cells. *BMC Vet. Res.* **15**, 248 (2019).
59. Lin, L. et al. TRIM21 restricts influenza A virus replication by ubiquitination-dependent degradation of M1. *PLoS Pathog.* **19**, e1011472 (2023).
60. Zhao, Z. et al. Tylvalosin exhibits anti-inflammatory property and attenuates acute lung injury in different models possibly through suppression of NF-κB activation. *Biochem. Pharmacol.* **90**, 73–87 (2014).
61. Wang, L., Dong, C., Chen, D. E. & Song, Z. Visceral pathology of acute systemic injury in newborn mice on the onset of Coxsackie virus infection. *Int. J. Clin. Exp. Pathol.* **7**, 890–904 (2014).

Acknowledgements

We thank Dr. Kenichi Yamamura (Center for Animal Resources and Development, Kumamoto University, Japan) for providing RBP4 knockout mice. We thank Dr. Yushan Zhu (Nankai University, China) and Dr. Lei Liu (Institute of Zoology, Chinese Academy of Sciences) for providing plasmids. We thank Dr. Gang Wang (Shandong Agricultural University, China) for helping to prepare PAMs. This study was supported by the Key Research and Development Program of Shandong Province (the Major Scientific and Technological Innovation Project, 2023CXGC010705) (Y.S. and J.L.) and the High-level Talents Recruitment Program of Shandong Agricultural University (Y.S.).

Author contributions

Q.H. and Y.S. conceived and designed research; Q.H. performed experiments and collected the data; H.Z. provided recombinant porcine RBP4 and contributed to animal experiments; Q.H., H.Z., and M.C. analyzed the data; W.X. helped to perform experiments. Q.H. and Y.S. wrote the manuscript; J.L. and L.S. revised the manuscript; Y.S. conceptualized the project and supervised the work.

Competing interests

The authors declare no competing interests.

Additional information

Supplementary information The online version contains supplementary material available at https://doi.org/10.1038/s42003-024-07052-1.

Correspondence and requests for materials should be addressed to Yingli Shang.

Peer review information *Communications Biology* thanks Hongbo Zhou and the other, anonymous, reviewer for their contribution to the peer review of this work. Primary handling editor: Christina Karlsson Rosenthal.